Distribution Agreement

In presenting this thesis or dissertation as a partial fulfillment of the requirements for an advanced degree from Emory University, I hereby grant to Emory University and its agents the non-exclusive license to archive, make accessible, and display my thesis or dissertation in whole or in part in all forms of media, now or hereafter known, including display on the world wide web. I understand that I may select some access restrictions as part of the online submission of this thesis or dissertation. I retain all ownership rights to the copyright of the thesis or dissertation. I also retain the right to use in future works (such as articles or books) all or part of this thesis or dissertation.

Signature:

Qingfeng Wang	Date

Potential energy surface and applications to carbon dioxide-water, carbon dioxide clathrate hydrate and hydrated HCl system

By

Qingfeng Wang
Master of Science

Chemistry

Joel M. Bowman, Ph.D
Advisor

Dr. Francesco A. Evangelista, Ph.D
Committee Member

Dr. Susanna L. Widicus Weaver, Ph.D
Committee Member

Accepted:

Lisa A. Tedesco, Ph.D
Dean of the James T. Laney School of Graduate Studies

Date

Potential energy surface and applications to carbon dioxide-water, carbon dioxide clathrate hydrate and hydrated HCl system

By

Qingfeng Wang
B.S., Xiamen University, 2015

Advisor: Joel M. Bowman, Ph.D

An abstract of
A thesis submitted to the Faculty of the
James T. Laney School of Graduate Studies of Emory University
in partial fulfillment of the requirements for the degree of
Master of Science
in Chemistry
2018

Abstract

Potential energy surface and applications to carbon dioxide-water, carbon dioxide clathrate hydrate and hydrated HCl system

By Qingfeng Wang

The potential energy surface is important to describe the molecular dynamics and molecular vibrations. In the first part of this thesis, an *ab initio*, full-dimensional, potential energy surface for CO_2-H_2O two-body interaction is presented. A full potential energy surface of dimer can be obtained by adding potentials for non-interacting monomers. Diffusion Monte Carlo calculations of the dimer zero-point energy are performed. Vibrational self-consistent and virtual-state configuration interaction method are used to characterize the vibrational eigenstates and energies. These results are in good agreement with experimental results. In addition, the CO_2-H_2O two-body potential energy surface is combined with existing water potential to develop a potential for the CO_2 clathrate hydrate. A computationally efficient local-monomer treatment for this clathrate hydrate is presented. In the second part of the thesis, the vibrational pre-dissociation of $HCl-(H_2O)_3$ cluster is studied. Using an existing potential energy surface, quasi-classical trajectory calculations were performed. This unimolecular decomposition can undergo two different pathways that were all observed by a large number of trajectory simulations. Information such as speed distribution, rotational energy distribution and branching ratio have been be obtained by analyzing final condition of the trajectories.

Potential energy surface and applications to carbon dioxide-water, carbon dioxide clathrate hydrate and hydrated HCl system

By

Qingfeng Wang
B.S., Xiamen University, 2015

Advisor: Joel M. Bowman, Ph.D

A thesis submitted to the Faculty of the
James T. Laney School of Graduate Studies of Emory University
in partial fulfillment of the requirements for the degree of
Master of Science
in Chemistry
2018

Acknowledgement

I would like to thank all the people who helped me make this dissertation possible due to their various contribution.

- Dr. Bowman is the key reason why this dissertation is possible. In the past two and half years he has been instructed me very kindly and finally offered me great opportunity to pursue the academic goal I longed for.
- I would like to thank Dr. Francesco A. Evangelista and Dr. Susanna L. Widicus Weaver for their time as committee.
- I thank my group members, Dr. Chen Qu, Dr. Xiaohong Wang, Dr. Hanchao Liu, Dr. Yimin Wang, Apurba Nandi, Brian Van Hoozen, especially Dr. Chen Qu for all the valuable discussions. I also thank Hanjie Jiang for nice cooperation on MSA package YouTube video development.
- I also thank Susan Browne Ann Dasher and Ana Maria Velez for various administrative suggestions and work.
- Last but not least, I should thank my parents for their unconditional love and support.

Table of Contents

List of Figures

List of Tables

Chapter 1 Introduction

1.1 Introduction

Theoretical chemistry examines the system of interest in the molecular level. Luckily, in principle, the behavior of molecules can be explained exactly under the quantum mechanics scheme. To be specific, the non-relativistic Schrödinger equation is a good enough formalism to contain all the useful information relevant to chemistry.

Unfortunately, the major barrier that prevents us from obtaining useful knowledge of molecular system is the notorious one, i.e., the lack of computational power to solve the Schrödinger equation accurately for molecules containing even moderate number of atoms. In order to reduce the computational difficulty of solving the Schrödinger equation, many approximations have been applied. The most popular method is a two-step strategy with the aid of Born-Oppenheimer approximation. It involves first constructing the potential energy surface, and in the second step obtaining useful information of molecule by evaluating the potential energy surface. In next two sections, the details of two steps and how are they related to my thesis will be explained.

1.2 Construction of the potential energy surface

In the first step, Born-Oppenheimer approximation is applied in order to solve the Schrödinger equation. This approximation takes the advantage of the fact that the mass of nuclei is much larger than the mass of electrons so that the motion of electrons can be adapted to the displacement of nuclei almost instantaneously. This is usually a very good and useful approximation. The computational difficulty has been reduced since the Schrödinger equation can be solved with fixed nuclei, preventing electrons

and nuclei moving simultaneously. As a result, one can solve the Schrödinger equation for different nuclear configurations. What is obtained in this step is called potential energy surface (PES). PES can be thought of a mathematical function $E(\boldsymbol{R})$ that gives energy of the molecular system E with the input of the position of atoms $\boldsymbol{R}$.

The PES can be constructed in several ways. The first method is to construct the PES on-the-fly. In principle, the PES can be obtained directly by solving the non-relativistic Hamiltonian with the Born-Oppenheimer approximation. The accuracy relies on the level of theory and basis applied. However, using the currently available computer power, only relatively low-level theory and small basis can be performed for even small molecular systems. The greatest advantage of this method is that it usually provides consistent and dependable result. That is to say it can describe the distorted system far away from its equilibrium configuration with reasonable accuracy up to the level of chosen theory and basis.

This method is used in Chapter 2 in order to generate a large number of CO_2-H_2O configurations that are physically reasonable. Notice the theory used for my 6-atom system is merely MP2 with basis VDZ.

A more widely used approach in our group for constructing PES is to fit an analytical PES. There are many different ways of formulating the analytical PES, as described in Chapter 2. The analytical PES typically used in our group is formulated as permutationally invariant polynomials with undetermined coefficients. This is also the PES I used in the rest of this thesis. Then, a large set of energies obtained from high-level *ab initio* calculation is used to fit those coefficients in PES. The fitting routine is a standard one developed in our group over many years. Technical details will be explained in Chapter 2. The greatest advantages for analytical PES is the speed of evaluation, which proves to be invaluable in computational-intensive calculations described in the section.

1.3 Application of the potential energy surface

In the second step of the procedure, useful information can be extracted by solving the Schrödinger equation of nuclei using PESs. This can be regarded as the application of PESs and also the main focus of this thesis. The application can be roughly categorized as molecular vibrations and dynamics simulations.

For molecular vibrations, one of the most basic applications is normal mode analysis, which assumes the potential is harmonic and modes are orthogonal. The result can be systematically improved using vibrational self-consistent filed (VSCF) and virtual-state configuration interactions (VCI). VSCF/VCI approach takes into account for the anharmonicity and mode-coupling. In our group, VSCF/VCI is realized by the code MULTIMODE, which contains a standard procedure to solve the Watson Hamiltonian. Diffusion Monte Carlo (DMC), which is used to obtain the exact anharmonic ground state energy, can also benefit from the efficient evaluation of PES. The idea of DMC is if one propagating the time-dependent Schrödinger equation along imaginary time $\tau = it$, then only the ground state lasts after long enough time.

The motion of molecules described by the time-dependent nuclear Schrödinger equation can be very expensive to solve. As a good approximation, when quantum effects are negligible, the motion of nuclei can be described by classical mechanics. Solving classical mechanics requires the numerical integration where PES is used. A better description is using quasi-classical trajectory (QCT) calculation. This simply means restrictions are applied on the initial condition for each atom so that the internal energy of molecules satisfies the rule of quantum mechanics. The rest of the propagation still follows the rule of classical mechanics. Details of application of QCT will be described in Chapter 3.

1.4 Overview of the thesis

This thesis contains three separate chapters.

Chapter 2 talks about the construction of a highly accurate PES and how to apply this PES to obtain anharmonic vibrational spectrum. This topic is mainly based on my published work.[1] We report an *ab initio*, full-dimensional, potential energy surface (PES) for CO_2-H_2O, in which two-body interaction energies are fit using a basis of permutationally invariant polynomials and combined with accurate potentials for the non-interacting monomers. This approach, which we have termed "plug and play" is extended here to improve the precision of the 2-body fit in the long range. This is done by combining two separate fits. One is a fit to 47593 2-body energies in the region of strong interaction and approaching the long-range and the second one is a fit to 6244 2-body energies in the long-range. The two fits have a region of overlap which permits a smooth switch from one to the other. All energies are obtained at the CCSD(T)-F12b/aug-cc-pVTZ level of theory. Properties of the full PES, i.e., stationary points, harmonic frequencies of the global minimum, etc., are shown to be in excellent agreement with direct CCSD(T)-F12b/aug-cc-pVTZ results. Diffusion Monte Carlo calculations of the dimer zero-point energy are performed and a dissociation energy, D_0, of 787 cm^{-1} is obtained using that ZPE, D_e and the rigorous ZPEs of the monomers. Using a benchmark D_e, D_0 is 758 cm^{-1}. VSCF/VCI MULTIMODE calculations of intramolecular fundamentals are reported and are in good agreement with available experimental results. Finally, the full dimer PES is combined with an existing *ab initio* water potential to develop a potential for the CO_2 hydrate clathrate $CO_2(H_2O)_{20}$(5^{12} water cage). A full normal-mode analysis of this hydrate clathrate is reported as are local-monomer VSCF/VCI calculations of the fundamentals of CO_2.

Chapter 3 is based on a joint experimental and theoretical work in order to understand the $HCl-(H_2O)_3$ vibrational predissociation. My contribution is to provide

QCT simulations complementing the experiment. As a result, only QCT-relevant contents will be discussed here. The cyclic HCl$-(H_2O)_3$ tetramer is the largest observed neutral HCl$-(H_2O)_n$ cluster. The vibrational predissociation (VP) of HCl$-(H_2O)_3$ is investigated by theory following the infrared (IR) excitation of the hydrogen-bonded OH-stretch fundamental. The energetically possible dissociation pathways are HCl + $(H_2O)_3$ (Pathway 1) and H_2O + HCl$-(H_2O)_2$ (Pathway 2). Bond dissociation energies, D_0, are calculated to be 2426 $\pm$ 23 cm^{-1} and 2826 $\pm$ 19 cm^{-1} for Pathway 1 and Pathway 2, respectively. Insights into the dissociation mechanism and lifetime are gained from QCT calculations, which are performed on a previously reported many-body potential energy surface. It is concluded that the dissociation lifetime is on the order of 10 ps and that the final trimer products are in their lowest energy cyclic forms.

Chapter 2 Construction and application of PES for CO_2−H_2O and extension to the hydrate clathrate

2.1 Introduction

The Force Field (FF) is a generic term that denotes an analytical representation of a potential describing the interactions of a molecule or a molecular cluster. The molecule may be as small as a triatomic or as a large as a huge covalently bound polymer. Molecular cluster is, as the name implies, a collection of molecules bound by weaker, non-covalent interactions. Typically, FFs for molecular clusters make use of the rigid-monomer approximation. This leads to a great simplification in the complexity/dimensionality of the FF. In the general case of flexible monomers, the FF is decomposed as a sum of intramolecular and intermolecular terms. The intramolecular terms are expressed as bond stretch and bending functions (often harmonic), and dihedral (torsional) interactions. The intermolecular interactions are expressed as Lennard-Jones or "exp-6" potentials, augmented by two-body multipole interactions, see for example "CHARMM".[2] More sophisticated FFs do account for many-body induced interactions as well, for example the "AMOBEA" water potential.[3] These interactions contain linear and non-linear parameters that are typically determined empirically, e.g., using known equilibrium structures, vibrational frequencies, thermodynamic properties, etc., or by using *ab initio* electronic energies to obtain the parameters fit some fitting procedure, a linear/non-linear least square optimization. Generally this approach does not provide precise fitting. Obtaining RMS fitting error with tens to hundreds of cm^{-1} is a typical result for FFs with flexible monomers. As a result structures and normal mode frequencies differ by few percent relative to

the *ab initio* results. Of course, by introducing more linear and non-linear parameters the fitting can be improved. Nevertheless, this approach has several limitations. One is the imposition of the models for intra and intermolecular interactions. This is especially true for intramolecular interaction, where harmonic models are often used. It is also true for the short-range parts of the intermolecular, which are represented by exponentials. Second, these FF representations generally do not describe three and higher-body interactions and they do not describe chemical reactions or isomerization (there are some exceptions, such as Reaxff[4]).

In the past decade or so, essentially model-free approaches to the analytical representation of potential energy surfaces have been developed and applied to numerous molecular systems including chemical reactions. These PESs are numerical fits to tens of thousands of high-level electronic energies. Ours in particular make use of fitting bases that are invariant with respect to permutations of like atoms. These general approaches have been reviewed[5–8] and the interested reader is directed to these.

A particular subset of these approaches, suitable for large molecular clusters governed by non-covalent interactions, has been developed by our group building on the seminal work of others,[9] albeit for rigid monomers. In the general approach for flexible monomers, the intermolecular interaction is represented by a many-body expansion; with the important 2 and 3-body fits obtained by the numerical approaches mentioned above. For example, for flexible water, these representations, which are high-dimensional, have been determined based on fitting tens of thousands of high-level electronic energies.[10,11] These representations of the water potential are transferable to other systems such as hydrate clathrates, as we have recently reported for the hydrate clathrates of H_2[12] and CH_4.[13,14] In these examples, 2 and 3-body, full-dimensional potentials were developed for H_2-H_2O and CH_4−H_2O and combined with the water potential and pre-existing high-level monomer potentials to obtain

the full PES. We have termed this approach wherein existing monomer potentials are combined with fitted 2 (and 3-body) potentials "plug and play".

All of these numerically based approaches produce highly precise fits, i.e., of the order of 10 to 100 cm^{-1} RMS fitting error, depending on the total energy span of the dataset. However, even a 10 cm^{-1} RMS fitting error would be considered large in the long-range part of the potential, where the interaction energies are of the order of tens of wavenumbers or less.

In this chapter, we report a new 2-body potential for CO_2−H_2O and combine it with high-level monomer potentials to obtain the full dimer PES. The approach described in those papers is extended here to greatly improve the precision of the 2-body PES in the long range, in recognition of the comments made above.

The CO_2−H_2O dimer has been extensively studied both experimentally and theoretically, as it is important for understanding the basis of many fundamental reactions such as photosynthetic conversion from CO_2 and H_2O to organic molecules. The complex has been proposed to be present in some planetary atmospheres.[15] In addition, the CO_2 hydrate clathrate, whose structure will be described later, has been proposed in the Martian atmosphere,[16–19] and also as a possible means to sequester CO_2.[20,21]

Early experiments on the CO_2−H_2O complex determined the minimum energy configuration. This was first reported by Peterson *et al.*, in a molecular-beam-electric resonance experiment.[22] With the determination of rotational constants, hyperfine spectra and dipole moments, it was shown that the global minimum geometry is of C_{2v} symmetry (Figure 2.4 (a)). Later, this result was confirmed and supported by further experiments.[23–25]

Many *ab initio* studies of stationary points and energetics of this complex have been reported over the past 40 years.[26–35] The complex is a challenge for theory because of the weak binding and the floppy nature of the stationary configurations. After several thorough studies using high-level methods, stationary points have now

been well-characterized,[34,36] and the early reports of two minima are not correct.

Developing an *ab initio*-based, full-dimensional, potential energy surface for the CO_2-H_2O complex is clearly desirable, albeit a challenge owing to the high dimensionality (12 vibrational degrees of freedom). Several PESs with rigid monomers, which reduce the dimensionality to 5, have been reported.[36,37] The most recent rigid-monomer PES was reported by Makarewicz in 2010.[34] This PES was a fit to roughly 23000 using MP2/aug-cc-pVTZ (plus bond-centered functions) energies, using a complex analytical expression that included damped long-range electrostatic and dispersion interactions. 168 non-linear parameters were optimized to obtain a precise fit. The reported unweighted RMS fitting error for 22500 configurations up to an energy of 3500 cm^{-1} is 11.8 cm^{-1}. This PES is certainly of high quality and can be used in a number of studies, but the limitation to rigid monomers certainly rules out applications to IR spectroscopy.

To the best of our knowledge, the only previous *ab initio*-based PES for flexible monomers was reported in 2005 by Wilcox and Bauer.[32] They used the conventional FF to represent this potential and it is worthwhile to recall this approach in detail. For the two intramolecular terms, they used following equations to represent CO_2 potential and H_2O potential:

$$\begin{aligned} E_{CO_2} = & \frac{1}{2}k_1(r_{C-O_1} - 1.16914)^2 \\ & + \frac{1}{2}k_1(r_{C-O_2} - 1.16914)^2 \\ & + \frac{1}{2}k_{12}(r_{O_1-O_2} - 2.33827)^2 \\ & + \frac{1}{2}k\delta(a_{OCO} - \pi)^2 \end{aligned} \tag{2.1}$$

$$
\begin{aligned}
E_{\mathrm{H_2O}} = & \frac{1}{2}k_1(r_{\mathrm{O-H_1}} - 0.96876)^2 \\
& + \frac{1}{2}k_1(r_{\mathrm{O-H_2}} - 0.96876)^2 \\
& + \frac{1}{2}k_{12}(r_{\mathrm{H_1-H_2}} - 1.52326)^2 \\
& + \frac{1}{2}k\delta(a_{\mathrm{HOH}} - 1.80917)^2,
\end{aligned}
\tag{2.2}
$$

where k_1, k_2, k_{12} and $k\delta$ are parameters, r_{ij} are 6 intramolecular bond lengths (three for each monomer) in Å and a_{OCO} and a_{HOH} are bond angles in radians. They expressed the intermolecular interactions with the form:

$$
E_{\mathrm{intermolecular}} = \sum_{i=1}^{n-\mathrm{set}} \sum_{j=1}^{9} C(i,j)(1/r_j)^i, \tag{2.3}
$$

where j represents 9 intermolecular atom-atom pairs. Here "$n-$set" determines the number of parameters. The best model has a RMS fitting error of 0.34 kcal/mol. and contains two minima, which are (incorrectly) present in the dataset of 172 G3(MP2)//B3LYP energies. The potential at the T-shaped global minimum is -2.84 and -3.18 kcal/mol for G3(MP2)//B3LYP and the force field, respectively. Another important limitation of the FF is that it is valid only for separations of the water oxygen and the carbon atom over the range of 2.0 to 8.0 Å. Thus, it cannot describe long-range interactions. Finally, given the limited range of energies in the dataset (up to 10 kcal/mol relative to separated monomers at equilibrium) it is unlikely that this force field could yield accurate anharmonic vibrational energies. In this context, the work of Chaban *et al.* is noteworthy.[15] This group reported anharmonic calculations of the monomer vibrational energies by obtaining electronic energies directly on grids and thus without recourse to an existing PES. We discuss these calculations in detail below.

The PES we report is based on fits to tens of thousands CCSD(T)-F12b/aug-cc-pVTZ 2-body interactions with flexible monomers. We use a fitting basis of permutationally invariant polynomials in so-called Morse variables. Details of this approach

have been given elsewhere[5,38] and so only a brief review of the essential aspects are given below. An important feature of the current approach is the use of two fits to create the final 2-body PES. One is a fit in the strong interaction region and in the moderate long-range region and the other is a fit for a much longer-range region. We denote these fits as "fit-SR" and "fit-LR". These two fits are then combined using a simple switching function to obtain the final 2-body PES. The 2-body PES is combined with previous 1-body monomer potential energy surface to obtain the full potential energy surface for the dimer. In addition, these monomer 1-body and 2-body potentials are combined with an accurate *ab initio* potential for water to develop a potential for CO_2 hydrate clathrates. These PESs are then used in a variety of anharmonic vibrational calculations.

The rest of the chapter is organized as follows. In Section 2.2, computational details of the *ab initio* calculations, fitting methods, diffusion Monte Carlo, VSCF/VCI calculations and the many-body representation of the CO_2 hydrate clathrate potential are given. Results and discussion are given in Section 2.3. These include an analysis of the PES, harmonic and VSCF/VCI vibrational energies for the dimer, followed by analyses of the hydrate clathrate calculation including a full normal-mode analysis and local monomer calculations of the fundamentals of intramolecular modes of the CO_2. Finally, a summary and conclusions are given in Section 2.4.

2.2 Theory and Computational Details

The "plug and play" approach[12–14] for CO_2–H_2O consists in writing the full potential as

$$V_{CO_2-H_2O} = V^{(1)}_{CO_2} + V^{(1)}_{H_2O} + V^{(2)}_{CO_2-H_2O} \tag{2.4}$$

where $V^{(1)}_{CO_2}$ and $V^{(1)}_{H_2O}$ are monomer potentials and $V^{(2)}_{CO_2-H_2O}$ is the intrinsic two-body potential. Hereafter, we refer this full potential as the "PES". The appeal of this approach is that the monomer potentials are pre-existing ones, which can be chosen

with a particular application in mind. For the present purpose, which is focused on vibrational dynamics, we selected monomer potentials that are of spectroscopic accuracy, when used in essentially exact vibrational calculations. Thus, the one for H_2O is from Partridge and Schwenke[39] and the one for CO_2 is from Huang *et al.*[40]

The objective is to obtain a full-dimensional potential energy surface for the $V^{(2)}_{CO_2-H_2O}$; we will refer to this as the "PES_{2b}". This is done by fitting a database of *ab initio* interaction energies obtained from three electronic structure calculations at a given nuclear configuration, one for the complex ($V_{CO_2-H_2O}$) and one each for the non-interacting monomers ($V^{(1)}_{CO_2}$ and $V^{(1)}_{H_2O}$). Because this interaction energy goes to zero as the monomers separate, the final PES_{2b} should faithfully reproduce this and also be as relatively precise in the long range as in the short range. In order to meet these requirements, PES_{2b} is a hybrid of two fits, which we denote fit-SR and fit-LR, and which are joined by a simple switching function. The first fit, as the name implies, is focused in the short to moderate long range while fit-LR is focused in the long-range and rigorously goes to zero as monomers separate.

2.2.1 *Ab initio* electronic energies databases

In order to sample the high-dimensional configuration space of interest, we first performed "*ab initio* molecular dynamics" calculations at the MP2/VDZ level of theory, with initial starting configurations at known stationary points and with initial kinetic energies ranging from 50 to 3000 cm^{-1}. From these calculations, roughly 21000 widely spread configurations were saved for higher level calculations of energies. Additional configurations were obtained based on the database of 23050 configurations used by Makarewicz[34] for rigid monomers. Those configurations were generated using grid method in the CO(water) distance (from 2 to 10 Å) and four angles specifying the orientation of the two rigid monomers. We used those configurations but with a small, random, displacement of a monomer bond length (±0.005 Å) or bond angle

($\pm 3^\circ$) at each. Finally, for the first generation data set, 1000 additional configurations were added along an approximate least-motion dissociation path and also a similar internal rotation path starting at the global minimum. In this way, first-generation database of roughly 45000 configurations was established.

Electronic energies at these configurations were obtained using the CCSD(T)-F12b theory[41,42] as implemented in MOLPRO,[43] with an aug-cc-pVTZ basis.[44,45] Based in part on a previous study, of CO_2-H_2O, where it was shown that the electronic binding energy using CCSD(T)-F12/VDZ was within 0.05 kcal/mol of the converged result (with respect to basis size),[35] no corrections to possible basis-set superposition errors were done.

After obtaining an initial fit (see below for details) using this database, unbiased diffusion Monte Carlo[46–48] calculations for the zero-point state of the complex were performed in order to explore of regions of the fit that might produce unphysical large negative values, i.e., "holes". A number of such "holes" were found and in their vicinity roughly 2000 electronic energies were added to the database. This database was used to obtain fit-SR (details given below). Finally, for fit-LR, 6244 long-range configurations were sampled with R_{CO} between 6 Å and 22 Å, where R_{CO} is the distance between carbon and the oxygen atom of H_2O. The database consists of all (1280) configurations and corresponding *ab initio* energies in the large database for fit-SR for R_{CO} is greater than 6 Å, plus 4964 additional configurations for R_{CO} in the range 6 to 22 Å for various internal configurations of the two monomers and relative orientations of the monomers.

2.2.2 PES_{2b} fitting

The approach to obtain fit-SR and fit-LR is the usual one we take, that is using a basis of permutationally invariant polynomials in Morse variables.[5] CO_2-H_2O is of the form $X_3Y_2Z_1$ and thus the full symmetric group is of order $3!2! = 12$. The Morse

variables are $y_{ij} = exp(-r_{ij}/\lambda)$ where r_{ij} is the internuclear distance between atom i and atom j and λ is a range parameter. For fit-SR λ is the (usual) value of 2.0 au. For fit-LR, after some optimization, a larger value, $\lambda = 7.0$ au, is used.

For fit-SR, the polynomial basis consists of a group of factored primary and secondary invariant polynomials,[5] namely

$$V(\mathbf{y}) = \sum_{\alpha=0}^{M} h_\alpha(\mathbf{p}(\mathbf{y}))q_b(\mathbf{y}), \tag{2.5}$$

where α is the total polynomial order of each term in the sum, starting from 0 to maximum order of M. Each order of polynomial itself is a summation of a series of symmetrized polynomials determined by polynomials h_a and secondary invariant polynomials q_b. Moreover, h_a is a polynomial of primary invariants $p(\mathbf{y})$. The number of $p(\mathbf{y})$ is equal to number of Morse variables, which is 15 for this six-atom system. In the present case, the maximum polynomial order is 6 which results in 5835 linear coefficients after expansion. The unknown coefficients were obtained using the standard least-squares method.

As was noted in the review on the above fitting method,[5] the above factored expression does not rigorously separate into non-interacting fragments in the corresponding asymptotic limit. Instead this asymptotic behavior is obeyed numerically by the fit. The reason for this non-separability and the remedy will become clear below, where we present a second permutationally invariant fitting method for fit-LR. This method is a modified version of monomial symmetrization (MSA).[5,38] In this approach the potential is represented in basis of symmetrized monomials, namely

$$V(\mathbf{y}) = \sum_{m=0}^{M} D_{\underline{l}} \mathcal{S}\left[\prod_{i<j}^{N} y_{ij}^{l_{ij}}\right], \tag{2.6}$$

where $N = 15$ is the number of Morse variables and $D_{\underline{l}}$ are the linear unknown coefficients. Each monomial is symmetrized by formal operator $\mathcal{S}$ based on the relevant permutation group.[5,38] Note, for a given maximum polynomial order the number of

unknown coefficients in the two approaches is equal, as the two approaches are formally equivalent. The modification mentioned above, is to "purify" the basis so that the expression rigorously goes to zero as the monomers separate.[12] This is done by eliminating terms in the basis that contain only intramolecular monomer Morse variables. For the long-range fit to the database of roughy 6000 electronic energies, the maximum polynomial order is 4, which results in 524 coefficients. The purification procedure eliminates 103 terms resulting in 419 coefficients finally.

Next to combine fit-SR and fit-LR to generate $\mathrm{PES_{2b}}$, we use a simple, finite-ranged switching function in the CO distance.[10,49–51] Thus,

$$\mathrm{PES_{2b}} = (1 - s(R_{\mathrm{CO}}))(\text{fit-SR}) + s(R_{\mathrm{CO}})(\text{fit-LR}), \tag{2.7}$$

where s is given by

$$s(R_{\mathrm{CO}}) = \begin{cases} 0, & \text{if } R_{\mathrm{CO}} < a \\ 10p^3 - 15p^4 + 6p^5, (p = \dfrac{R_{\mathrm{CO}} - a}{b - a}) & \text{if } a \leq R_{\mathrm{CO}} \leq b \\ 1, & \text{if } R_{\mathrm{CO}} > b \end{cases} \tag{2.8}$$

Thus, s is a smooth function that varies from 0 to 1 in the switching region $[a, b]$. Notice that $\mathrm{PES_{2b}}$ will be reduced to fit-SR when $R_{\mathrm{CO}} < a$ and fit-LR when $R_{\mathrm{CO}} > b$. In the present application the switching region is from 5 to 6 Å. This range was determined empirically by inspecting potential cuts in R_{CO}, as shown below, and locating a region where the cuts from the two fits overlap well.

2.2.3 Dissociation energy and vibrational analysis of the CO_2−H_2O dimer

The rigorous zero-point energy (ZPE) was obtained using the unbiased diffusion Monte Carlo (DMC) method.[46–48] In brief, this method uses a stochastic approach to solve the Schrödinger equation in imaginary time in Cartesian coordinates. The long-time solution decays to the zero-point state and thus the method provides a way of obtaining both the wavefunction and energy of this state. In our application,

10 DMC trajectories were run for both the complex and the monomers. For each trajectory 30000 walkers were propagated for 50000 steps, with the last 40000 used to determine the wavefunction and zero-point energy. The number of potential calls per trajectory is of the order of 10^{10}, and clearly a PES is essential for this approach. Even with a PES, the CPU effort for these calculations is of the order a couple of days on a single node of a workstation. With these rigorous ZPEs, combined with an accurate electronic dissociation energy, D_e, a rigorous dissociation energy D_0 was determined.

For excited vibrational states, the code MULTIMODE[52–56] was used to perform vibrational self-consistent field (VSCF) and virtual state configuration interaction (VCI) calculations.[56,57] There are 12 vibrational modes of this floppy complex and an exact treatment of all of these are beyond the current state of the art. Thus, we restrict attention to the seven intramolecular modes. Even with this reduction, the potential is 7-dimensional and doing numerical quadratures of matrix elements in this dimensionality would be very compute intensive. To overcome this problem, MULTIMODE uses a hierarchical n-mode representation of the potential.[52] Based on many previous calculations, a 4-mode representation (4MR) of the potential should produce results that are converged to within a few wavenumbers or less. With this 4MR, the maximum quadrature dimensionality is 4; however, there are $\frac{7!}{4!3!}$=35 4-mode grids. For the basis, a direct-product is used and the single-mode basis consists of an underlying primitive basis of 12 harmonic-oscillator functions. In the VCI calculation, the excitation space consists of single, double, triple and quadruple excitations, with the sum of quanta for these levels of excitations being 12, 11, 10 and 9, respectively. This resulted a VCI matrix of order 26496, which is readily diagonalized.

2.2.4 CO_2 hydrate clathrate

There is great interest in CO_2 hydrate clathrates with a corresponding extensive literature and it is certainly beyond the scope of this paper to review this literature. Our purpose here is to illustrate how the new CO_2−H_2O PES can be used to develop many-body potential for these clathrates. We do note that there have been several studies of the dynamics of CO_2 in water cages making use of empirical interaction potentials.[58,59] Density functional theory, B3LYP/6- 31G(d), was used to obtain the optimum and maximum cage occupancy for five different cages.[60]

The lack of an *ab initio*-based clathrate model motivates us to construct a many-body-representation based high quality PES for CO_2 hydrate clathrate. Thus, we use the well-known many-body representation of the potential given by

$$\begin{aligned} V_{\mathrm{CO_2@(H_2O)_n}} \approx\, & V^{(1)}_{\mathrm{CO_2}} + \sum_{i=1}^{n} V^{(1)}_{\mathrm{H_2O}(i)} \\ & + \sum_{i=1}^{n} V^{(2)}_{\mathrm{CO_2-H_2O}(i)} + \sum_{i=1}^{n}\sum_{j=i+1}^{n} V^{(2)}_{\mathrm{H_2O}(i)-\mathrm{H_2O}(j)} \\ & + \sum_{i=1}^{n}\sum_{j=i+1}^{n}\sum_{k=j+1}^{n} V^{(3)}_{\mathrm{H_2O}(i)-\mathrm{H_2O}(j)-\mathrm{H_2O}(k)} \\ & + V(\text{higher order water potential terms}), \end{aligned} \tag{2.9}$$

where n is the number of water molecules. For the water potential, we use the accurate, *ab initio* MB-pol potential,[11] which also uses the Partridge-Schwenke H_2O monomer potential. (We used this many-body representation for the CH_4 hydrate clathrate,[14,61] with the *ab initio* WHBB water potential.[62])

The above representation is restricted to 2-body CO_2-H_2O(i) interactions and we use the one we are reporting here. In line with numerous previous studies, we expect the 3-body interaction $V^{(3)}_{\mathrm{CO_2-H_2O}(i)-\mathrm{H_2O}(j)}$ to be much less than the 2-body $V^{(2)}_{\mathrm{CO_2-H_2O}(i)}$ one. However, in a hydrate clathrate there are more 3-body interactions than 2-body ones, so it is necessary to examine the total interaction in detail. Thus, we calculated these two potentials at the optimized global minimum geometry of $CO_2(H_2O)_{20}$ at

the MP2/aVTZ level of theory. For this hydrate clathrate, there are 20 $V^{(2)}_{CO_2-H_2O(i)}$ terms and 190 $V^{(3)}_{CO_2-H_2O(i)-H_2O(j)}$ terms, and average potential for each three-body term is -0.53 cm^{-1} while average potential for each two-body term is -189.16 cm^{-1}. As a result, the total 3-body potential is about 2.7% of the total 2-body potential. So we can safely ignore the 3-body interactions in this study, which focuses on the global minimum of this hydrate clathrate. Finally, we denote this many-body potential as PES-CW20, as "C" stands for "Carbon dioxide" and "W" for "Water".

Two vibrational analyses of $CO_2@(H_2O)_{20}$ are done, following a geometry optimization. One is a full normal-mode analysis of the hydrate clathrate and the second one is a VSCF/VCI local monomer (LMon) analysis of the embedded CO_2. In the LMon approach,[62] the motion of flexible CO_2 is considered with the full interaction of the water molecules, which are fixed at their reference configurations at the minimum of the hydrate clathrate. In this approach, a normal-mode analysis is done for the embedded CO_2; we refer to this as "local normal-mode" analysis. This yields 9 non-zero frequency modes, five of which are frustrated rotation and translational modes and 4 are the intramolecular modes. MULTIMODE VSCF/VCI calculations are done using the 9 local modes and also the 4 intramolecular modes. For both, a 4MR of the potential is used. For these calculations, each single mode function is represented by a basis of 9 harmonic-oscillator wave functions. In the VCI calculation, the excitation space again consists of single, double, triple and quadruple excitations, with the sum of quanta for these levels of excitations being 9, 8, 7 and 6, respectively. The VCI matrices are of order 24310 and 715 for the 9-mode and 4-mode calculations, respectively.

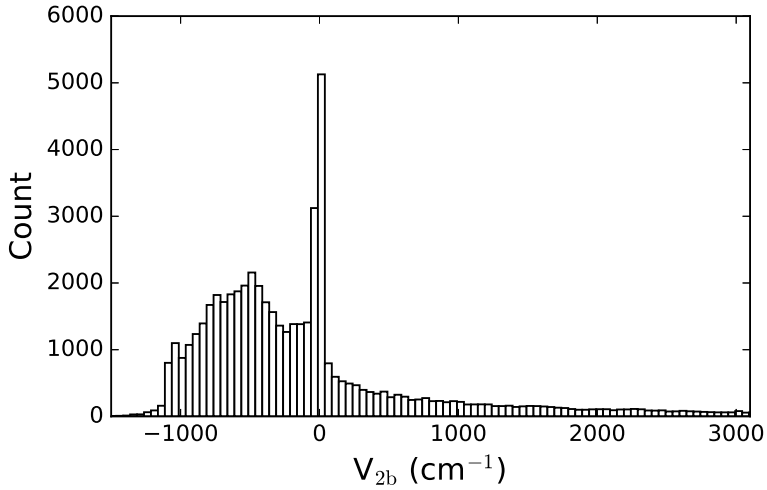

Figure 2.1: Histogram distribution of 2-body energies V_{2b} from the combined datasets (roughly 53000 energies) for fit-SR and fit-LR. Bin width is 50 cm^{-1}.

2.3 Results and Discussion

2.3.1 PES_{2b} fitting precision

The distribution of 2-body energies is shown in Figure 2.1. As seen, there is a concentration of energies around 0 cm^{-1}. This comes mostly from the fit-LR database Also, a majority of energies are negative and this is mainly due to AIMD sampling, which favors configurations with low potential energy. The cut-off at around -1000 cm^{-1} is a rough indication of the electronic binding energy of the dimer. The positive 2-body energies are indicative of repulsive interactions, which must be included to obtain a global 2-body PES.

The RMS fitting error for fit-SR to the full database of roughly 48000 energies is 6.3 cm^{-1} and the one for fit-LR is 0.40 cm^{-1}. The cumulative RMS with negative energies is 5.17 cm^{-1} (34119 configurations) for fit-SR and 0.32 cm^{-1} (4890 configurations) for fit-LR. This clearly indicates precise fitting, especially for the long-range fit. Thus, the objective of obtaining a small RMS fitting error for the long-range has been achieved. In addition, fit-LR goes to zero rigorously as the monomers separate.

We next examine the two fits and direct *ab initio* calculations for three cuts as

a function of R_{CO} in Figure 2.2. As seen, and as expected, fit-SR matches the *ab initio* energy very well up to about 6 Å while fit-LR is almost identical to *ab initio* energies from 6 Å. Also, and of direct relevance to the switch between these two fits, we see that the two fits are in very good agreement in the range 5 to 6 Å. Thus, the switching region is 5 to 6 Å.

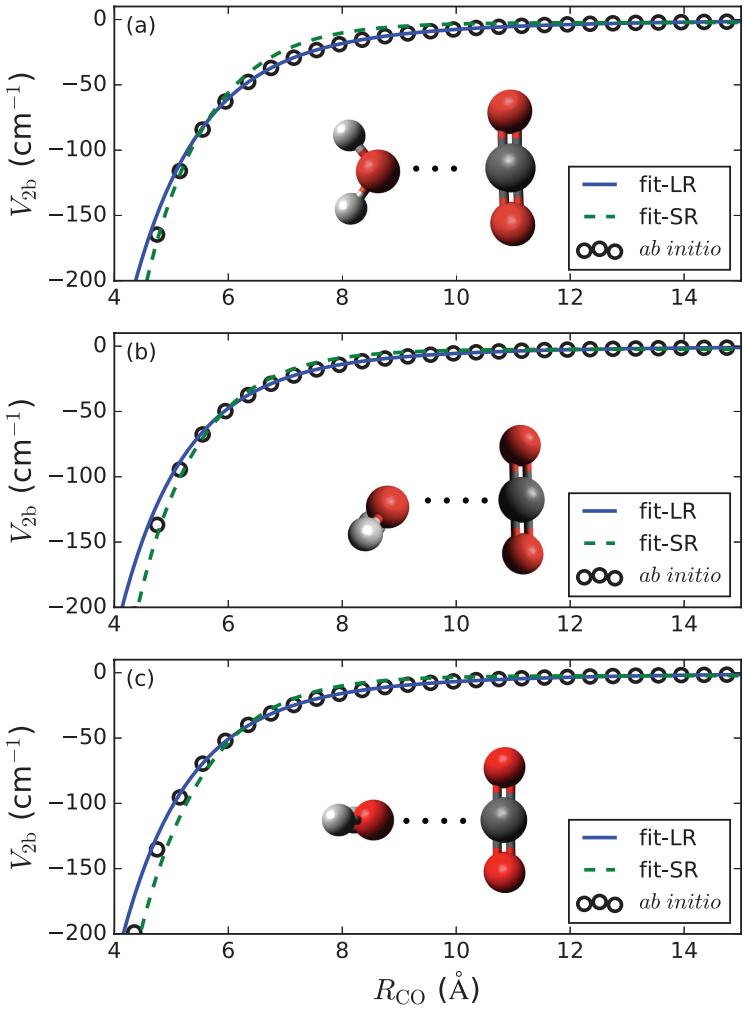

Figure 2.2: Rigid monomer dissociation cuts starting from the equilibrium structure along R_{CO} direction. Panel (a)-(c) corresponds to geometries in Figure 2.4 (a)-(c).

The accuracy of the repulsive interaction between CO_2 and H_2O in the fitted PES_{2b} is also important to examine. This is done in Figure 2.3 for the indicated monomer orientation, where good agreement with direct *ab initio* energies is seen.

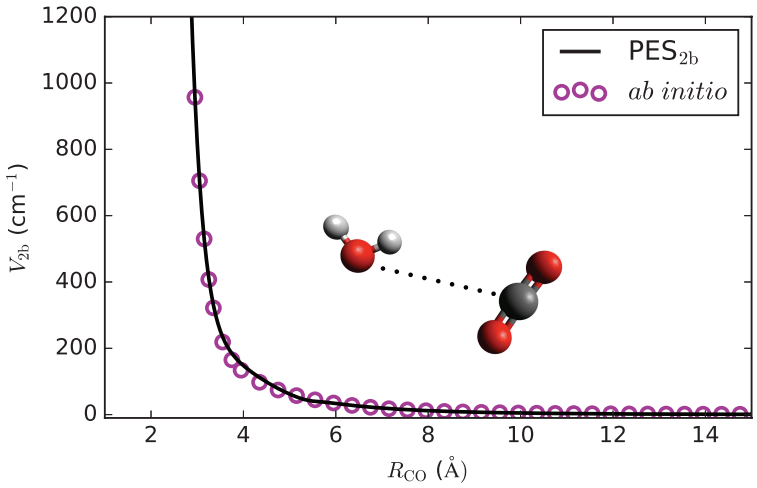

Figure 2.3: Rigid monomer potential cut versus R_{CO} for the indicated repulsive configuration.

2.3.2 Properties of the CO_2–H_2O PES

Stationary points of the full PES were obtained by applying Newton's method. The global minimum and four saddle point geometries are shown in Figure 2.4. We confirm the earlier finding of Makarewicz[34] that there is only one minimum configuration, denoted here as i.e., "a". In "a", the bond length for water in the complex is the same as the isolated monomer, the bond angle increases slightly to 105.1°. In addition, CO_2 is no longer linear in global minimum; instead, the O=C=O angle is 178.1° with C=O bond pointing away from H_2O. Note, R_{CO} for "a" is 2.7552 Å at the CCSD(T)/CBS(CP,AV5Z/AV6Z) level of theory;[35] the PES value of 2.753 Å is in good agreement with this benchmark value.

The PES stationary configuration energies are given in Table 2.1, along with present CCSD(T)-F12b/aVTZ *ab initio* calculations. The electronic dissociation energy D_e of "a" from the MP2/aVTZ PES[34] is 1004 cm^{-1} and the benchmark CCSD(T)/CBS(CP,AV5Z/AV6Z) value is 1024.8 cm^{-1}.[35] Thus, the PES value is in error by 28 cm^{-1}. The PES saddle point energies "b" to "e" are in excellent

Table 2.1: Energies of stationary points from indicated sources. Note for the energy of configuration "a", the global minimum, is referenced to the isolated monomers and has the value of -D_e while all energies of other configurations are referenced to "a".

	a	b	c	d	e
CCSD(T)-F12b/aVTZ	-1054	297	332	619	877
PES	-1053	302	328	616	876
MP2/aVTZ PES[34]	-1004	291	308	635	828

agreement with directly calculated ones and the corresponding values from the rigid-monomer MP2/aVTZ-based PES[34] are in reasonable agreement with the present energies.

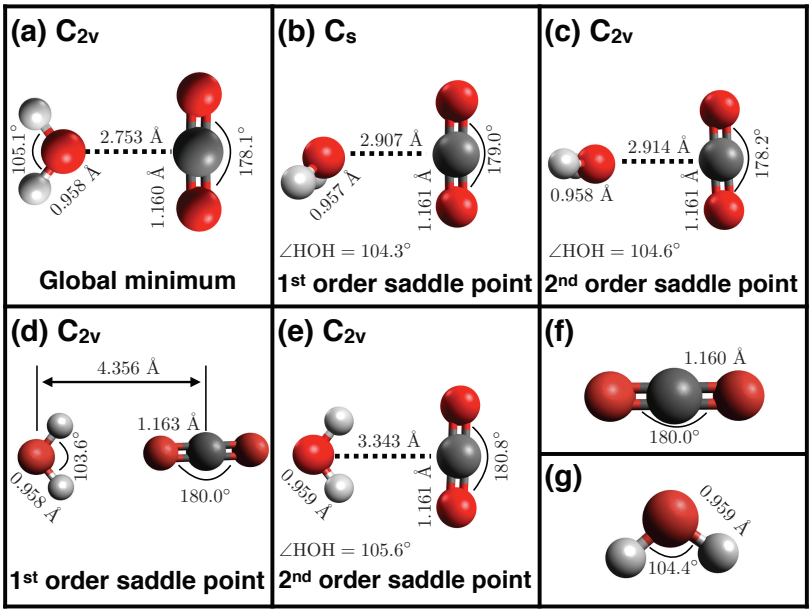

Figure 2.4: (a) to (e) are geometries of saddle points obtained from PES. Selected bond lengths and angles are shown directly in the figure. (f) and (g) are monomer global minimum configurations obtained from monomer PESs. Note that our geometry (d) and (e) correspond to geometry (f) and (d) respectively in Makarewicz's paper.[34]

The fixed global minimum-configuration and relaxed monomer dissociation and internal rotation cuts from the PES are shown in Figure 2.5 and Figure 2.6, respectively. As expected, the fixed-monomer dissociation energy is larger than the relaxed one, although the difference is small. There is a larger difference between the fixed and relaxed internal rotation barrier. These barrier heights are in reasonable agreement

with empirically determined ones 305.36 ± 0.5 cm^{-1} (fixed) and 285.66 ± 1.4 cm^{-1} (relaxed).[63] It is noteworthy that in the same research the R_{CO} distance was reported 2.83 Å which is 0.08 Å longer than the benchmark distances. Since there is relatively large discrepancy in bond length between their and our research, it should not surprise us if there is also some discrepancy in internal rotation barriers.

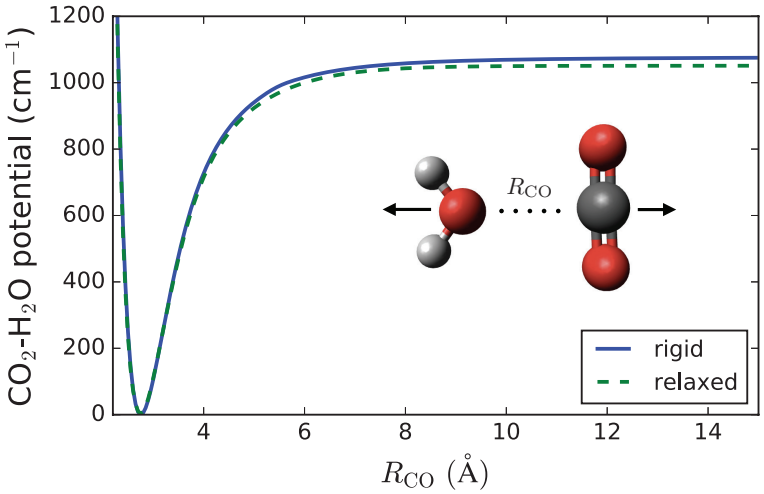

Figure 2.5: Relaxed cut and rigid cut comparison for dissociation path. Relaxed cut converges to 1053 cm^{-1} while rigid cut converges to 1077 cm^{-1}. Both cuts have the same global minimum.

The dissociation energy D_0 was obtained from D_e and the following DMC ZPEs: 2534.8 ± 1.1 cm^{-1} for CO_2, 4634.2 ± 1.2 cm^{-1} for H_2O and 7435.8 ± 1.9 cm^{-1} for CO_2−H_2O. Thus, D_0 equals 787 cm^{-1} using a D_e of 1053 cm^{-1} and 758 cm^{-1} using the benchmark D_e. Unfortunately, no experimental value has been reported.

Harmonic frequencies of the global minimum obtained from both *ab initio* CCSD(T)-F12b/aVTZ calculations and the PES are presented in Table 2.2. Before comparing these in detail, it should be kept in mind that the full PES is not a fit to CCSD(T)-F12b/aVTZ, but a composite consisting of a fit of 2-body CCSD(T)-F12b/aVTZ energies plus previous, spectroscopically accurate monomer potentials. With this in mind, we note some differences for some of the low frequency intermolecular modes.

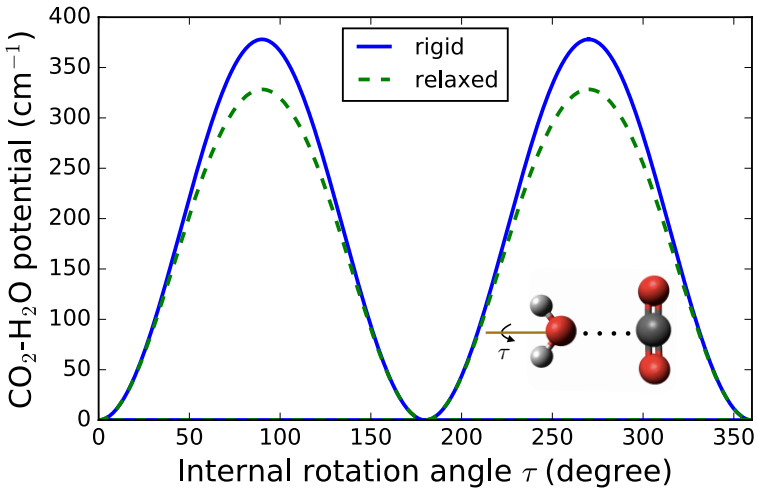

Figure 2.6: Relaxed cut and rigid cut comparison for internal rotation. Relaxed cut has peak height 328.0 cm^{-1} while rigid cut has peak height 378.1 cm^{-1}. Both cuts have the minimum potential 0 when water plane is in the same plane as CO_2 plane ($\tau = 0°$) and have the maximum potential when water plane is perpendicular with CO_2 plane ($\tau = 90°$). τ is the torsion angle formally defined by the angle between normal vectors of CO_2 and H_2O plane. In this particular internal rotation cut, τ happens to be the angle rotating water about C_{2v} axis counterclockwise.

There is a relatively big discrepancy for $\nu_{\text{int}}(1)$. One possible explanation is that global minimum geometries used for NMA are not identical for PES and *ab initio* calculation. Since low-frequency intramolecular mode is more sensitive to geometric change than intermolecular modes, NMA calculated for PES and *ab initio* could also be different. For the intramolecular modes the PES results are within a few wave numbers of the *ab initio* results. Also, the PES results are in very good agreement with previous CCSD(T)-F12b/VTZ results.[35] Note that mode (3) is essentially the R_{CO}-stretch. The harmonic frequencies of the isolated monomers are given in parentheses next to the corresponding frequency in the dimer to indicate how these change in the dimer. For CO_2 the degeneracy of the bend (at 673 cm^{-1}) is lifted in the dimer and, not surprisingly, the two frequencies, i.e., $\nu_{b1}(CO_2)$ and $\nu_{b2}(CO_2)$, straddle the isolated CO_2 one. With the notable exception of this bending mode, the monomer harmonic frequencies are only slightly changed upon complexation.

Table 2.2: Harmonic frequencies of CO_2−H_2O and isolated monomers (in parentheses) calculated directly using CCSD(T)-F12b/aVTZ theory and labeled "*ab initio*" and from the PES. $\nu_{\text{int}}(3)$ and $\nu_{\text{int}}(4)$ correspond to R_{CO} and τ intermolecular displacements, respectively.

Mode Symbol	*ab initio*	PES
$\nu_{\text{int}}(1)$	46	2
$\nu_{\text{int}}(2)$	75	55
$\nu_{\text{int}}(3)$	118	116
$\nu_{\text{int}}(4)$	174	149
$\nu_{\text{int}}(5)$	178	171
$\nu_{b1}(CO_2)$	664(673)	664
$\nu_{b2}(CO_2)$	678(673)	678
$\nu_{\text{sym}}(CO_2)$	1353(1352)	1355
$\nu_{b}(H_2O)$	1646(1648)	1645
$\nu_{\text{asym}}(CO_2)$	2394(2393)	2400
$\nu_{\text{sym}}(H_2O)$	3835(3835)	3829
$\nu_{\text{asym}}(H_2O)$	3945(3944)	3951

VSCF/VCI fundamental frequencies, calculated from MULTIMODE, are compared with experimental and other theoretical results in Table 2.3. Note, that there are two entries for the $\nu_{\text{sym}}(H_2O)$ with a small, i.e., 3 cm^{-1}, difference in energies. An

examination of the VCI expansion coefficients reveals some mixing with a combination state consisting of one quanta of excitation each of the following: the lower-energy CO_2 bend $\nu_{b1}(CO_2)$, the symmetric CO_2 stretch and the H_2O bend. This state is close in energy to the $\nu_{\rm sym}(H_2O)$ state and so mixing is not a surprise. (In first order, this mixing requires a 4-mode coupling matrix element.) Overall, the present results are in very good agreement with experiment, especially the ones using the Ne matrix. Also, they are substantially closer to experiment than the previous calculations. This is probably mostly due to the higher level of *ab initio* theory used in the present calculations. However, the previous vibrational calculations were done using second-order perturbation theory corrections to VSCF energies and restricted to pairwise coupling of modes and so they are not as rigorous as the present ones. Finally, note that bending modes of CO_2 are strongly split and there is virtually no Fermi resonance affecting the CO_2 symmetric stretch.

Mode	MULTIMODE	MP2/aVTZ[15]	Ne matrix[64]	N_2 matrix[65]
$\nu_{b1}(CO_2)$	660	647	658.7	656.4
$\nu_{b2}(CO_2)$	676	659	672.2	665.3
$\nu_{\rm sym}(CO_2)$	1285	1311	Not IR active	Not IR active
$\nu_b(H_2O)$	1583	1487	1595.2	1597.0
$\nu_{\rm asym}(CO_2)$	2348	2366	2348.2, 2348.8	2351.1
$\nu_{\rm sym}(H_2O)$	(3661, 3664)	3550	3664.8	3634.7
$\nu_{\rm asym}(H_2O)$	3759	3634	3760.3, 3754.5	3727.3

Table 2.3: Comparison of fundamental frequencies of CO_2-H_2O calculated from MULTIMODE, previous 2-mode anharmonic calculations and two matrix isolation experiments.

2.3.3 Application to $CO_2@(H_2O)_{20}$

The fully optimized $CO_2@(H_2O)_{20}$ geometry is shown in Figure 2.7. The CO_2 bond angle is 179.8° and both bond lengths are 1.160 Å. These values are very close to isolated CO_2 at equilibrium. The distances between C and the oxygen atoms in the surrounding water molecules are in the range 3.5-4.0 Å, substantially larger than this distance at the dimer minimum. So, clearly the equilibrium structure in

the cage is a trade-off between attractive and repulsive interactions with the water molecules. Also, the orientation of the CO_2 bond axis is essentially perpendicular to and centered with respect to a pentagonal face.

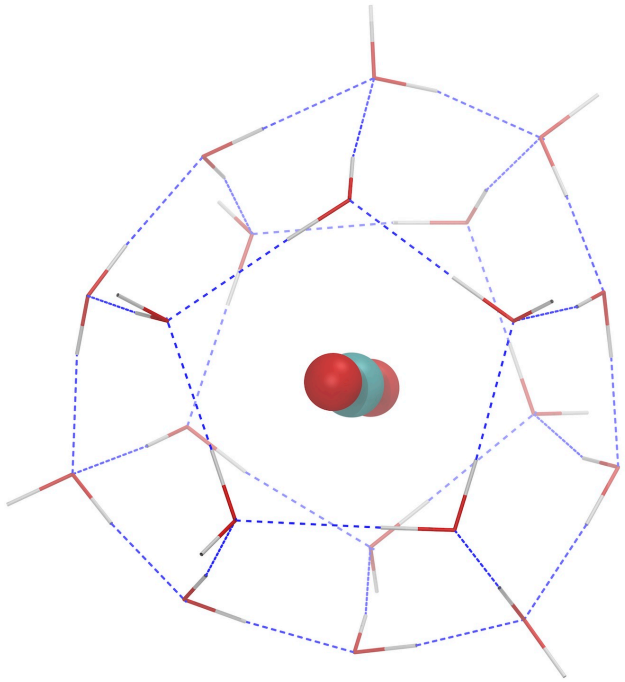

Figure 2.7: Global minimum of flexible $CO_2@(H_2O)_{20}$.

From this minimum we obtained an estimate of the electronic dissociation energy of 3799 cm^{-1} for CO_2 by using the same geometry for the $(H_2O)_{20}$ as for the global minimum and for CO_2 removed. We also examined the least-motion path of the CO_2 moving out of the cage through the center and perpendicular to the pentagonal face, with the water molecules held fixed. The barrier obtained is more than 20000 cm^{-1} and so clearly it would be necessary to open the pentagonal face for the CO_2 to escape. In fact, this has been seen for the 5^{12} cage, in recent molecular dynamics calculations, using an empirical potential.[59]

Figure 2.8 is a contour plot of the rotational potential for CO_2 at the global minimum position. For simplicity CO_2 was set to be linear and the z-axis is the bond

axis and the two angles θ and ϕ are the usual polar angles. The figure shows the barrier is not small so the orientation of CO_2 is locked somewhat toward one of the pentagonal faces. The potential does have quasi-periodicity as there are twelve such faces (which, however, are not identical).

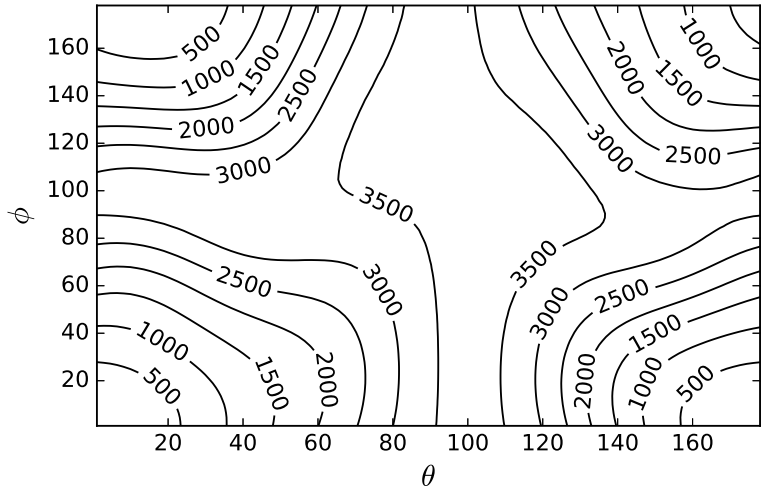

Figure 2.8: Contour plot of the CO_2 rotational potential (in cm^{-1}) at the global minimum of $CO_2@(H_2O)_{20}$ in the polar angles θ and ϕ (in degrees). The energy is referenced to global minimum, where θ and ϕ are zero.

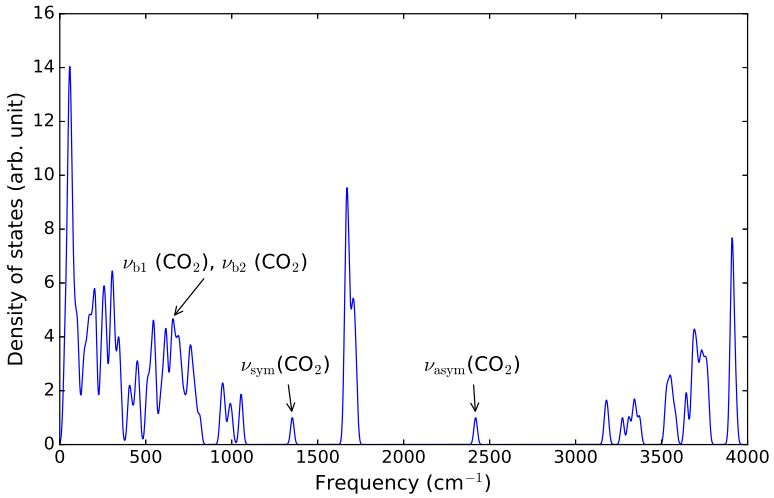

Figure 2.9: Vibrational density of states of $CO_2@(H_2O)_{20}$ calculated using full-dimensional normal-mode analysis. Four high frequency intramolecular vibrations of CO_2 are labeled.

Table 2.4: 4-mode, 9-mode VSCF/VCI local-monomer vibrational energies and LMon and full harmonic frequencies (cm^{-1}) of the CO_2 monomer in $CO_2@(H_2O)_{20}$.

Mode	4-Mode	9-Mode	LMon NMA	Full NMA
frustr-trans	-	59	55	30
frustr-trans	-	61	59	37
frustr-rot	-	71	69	26
frustr-rot	-	74	72	85
frustr-trans	-	76	73	87
$\nu_{b1}(CO_2)$	654	656	660	655
$\nu_{b2}(CO_2)$	657	659	663	655
$\nu_{sym}(CO_2)$	(1292, 1359)	(1294, 1363)	1353	1352
$\nu_{asym}(CO_2)$	2356	2356	2418	2418

We performed a full normal-mode analysis of the $CO_2@(H_2O)_{20}$ and a smoothed density of states is plotted in Figure 2.9. The smoothing was done by replacing each normal mode frequency (represented say by a stick of constant height) by a Gaussian curve with full-width half maximum of 10 cm^{-1}. Notice, under such resolution, the two CO_2 bending modes $\nu_{b1}(CO_2)$ and $\nu_{b2}(CO_2)$ are indistinguishable. Further, these modes are embedded in a similar spectral range of water cage modes suggests that some coupling of the CO_2 bending modes with cage modes is possible. However, an examination of the normal mode vectors shows this not to be the case. The symmetric and asymmetric CO_2 stretch modes are clearly isolated. So, this all suggests that a local monomer treatment of the CO_2 intramolecular vibrational modes should be reasonable. This is verified in Table 2.4, where the local-monomer harmonic frequencies of CO_2 are compared with corresponding results from the full normal-mode analysis. There are larger differences for the bend modes than the stretches, and this is understandable, based on the preceding discussion of the vibrational density states.

VSCF/VCI vibrational energies using just the four high-frequency intramolecular modes and all (9) local monomer modes are given in this table as well. As seen, there is very good agreement between these two set of results, implying little coupling between 5 low-frequency modes and 4 high-frequency modes. Both sets of calculations find strong mixing between the symmetric stretch with the bend which results in a Fermi-

diad , analogous to the isolated gas-phase Fermi-diads at 1286 and 1383 cm^{-1}. These Fermi-diads have been observed in a room temperature Raman spectrum of CO_2 in the larger $5^{12}6^2$ hydrate clathrate at roughly 1277 and 1382 cm^{-1},[66] values that are close to the gas-phase ones. The present calculations show an up-shift of the lower-energy diad and a down-shift of the higher energy one, relative to these experimental results, which unfortunately are not directly comparable to the present calculations. The calculated CO_2 asymmetric stretch at 2356 cm^{-1} is in good agreement with an experimental value of 2347 cm^{-1}, obtained in IR reflectance spectra of CO_2 in the smaller of two clathrate hydrates.[67]

Finally, comparing VSCF/VCI calculations for $CO_2@(H_2O)_{20}$ shown in Table 2.4 with calculations for CO_2-H_2O system in Table 2.3, one can find that two bending modes are much less separated in $CO_2@(H_2O)_{20}$. The energy separation is about 14-16 cm^{-1} for CO_2-H_2O while it is only about 1-3 cm^{-1} for $CO_2@(H_2O)_{20}$. Also, the symmetric stretch is not strongly perturbed by the bend in the dimer, where it is in the hydrate clathrate. The reason for these significant differences is likely because the CO_2-H_2O interaction is much stronger in the dimer than in the hydrate clathrate (recall the differences in the distance) in the two so the perturbation is smaller. In addition, the anisotropy is much less in $CO_2@(H_2O)_{20}$ since CO_2 is perturbed roughly uniformly from all directions. Five non-zero low-frequency modes shows that CO_2 is unable to rotate or translate freely in the water cage. It is noteworthy that in full-scale normal-mode analysis, these five frustrated rotational and translational modes plus two bending modes are all coupled significantly with water cage movements so that the local-monomer model cannot recover them accurately.

2.4 Summary and conclusions

In this chapter, I presented an accurate, full-dimensional, 2-body potential energy surface for CO_2-H_2O. This potential energy surface is a hybrid of two fits, denoted

fit-SR and fit-LR linked by a switching function. fit-SR is a permutationally invariant fit to 47593 *ab initio* energies of CCSD(T)-F12b/aVTZ level theory. fit-LR is also a permutationally invariant fit to 6244 CCSD(T)-F12b/aVTZ electronic energies, that rigorously goes to zero in the long range and which has an RMS fitting error of 0.4 cm^{-1} . This 2-body potential energy surface is combined with previous spectroscopically accurate potentials for the monomers to produce the final potential energy surface. The utility of this 2-body potential was demonstrated by using it, together with a previous water potential, to develop a potential for the small CO_2 hydrate clathrate $CO_2@(H_2O)_{20}$. Numerous properties of these potentials, including stationary points, harmonic frequencies, etc., were reported. The rigorous dissociation energy, D_0, of the dimer was reported as 787 cm^{-1} using the 2-body PES D_e of 1053 cm^{-1} and 758 cm^{-1} using the benchmark D_e. The latter value is then the current benchmark number for this important dimer. VSCF/VCI coupled-mode calculations of vibrational fundamentals were reported for the seven intramolecular modes of the dimer and the local-normal modes of CO_2 in the hydrate clathrate, using a 4-mode representation of the potential for both sets of calculations. These were compared, with no scaling or empirical adjustments, with available experimental results and agreement within a few wavenumbers was seen.

In summary, the new 2-body potential is a major step forward in providing both a highly accurate and transferable potential that should see many future applications.

2.5 CO_2-H_2O software package

See supplementary material of the published paper[1] for details on downloading the software to evaluate the 2-body potential energy surface.

Chapter 3 Vibrational predissociation of $HCl-(H_2O)_3$

3.1 Introduction

Water-hydracid complexes are prototype systems for the study of hydrogen bond (H-bond) properties and the mechanisms of acid solvation. The unique properties of water arise from its ability to form H-bonds, which often leads to the stabilization of intermediates, the shifting of molecular vibrational energies, and the lowering of activation barriers for reactions.[68,69] The ability of water to stabilize ions is also well known;[70] however, a detailed understanding of the dynamics leading to acid ionization within mixed clusters is uncertain. A bottom-up approach aims to identify trends in H-bonds dissociation through isolation of small mixed clusters. This starts with dimers containing one water and one hydrogen halide species, and then sequentially adding solvent water molecules to compare properties of larger cyclic networks. This chapter focuses on the vibrational predissociation (VP) of the $HCl-(H_2O)_3$ tetramer (referred to henceforth as HWWW), the largest neutral $HCl-(H_2O)_n$ cluster observed without ionization to the acid. Addition of one or two water molecules to this mixed cluster is expected to initiate proton migration to generate a stable solvent ion pair.[71–78] Although the existence and structure of the HWWW tetramer was debated in the past, the most recent calculations confirm that it is stable and its optimized geometry is cyclic, as shown in Figure 3.1.[71,79–82]

An investigation of this mixed cluster is also interesting because there are two close-lying dissociation channels that can be accessed by excitation of the intramolecular OH-stretch fundamentals, yielding HCl (Pathway 1, Equation 3.1) or H_2O (Pathway 2, Equation 3.2) monomer fragments:

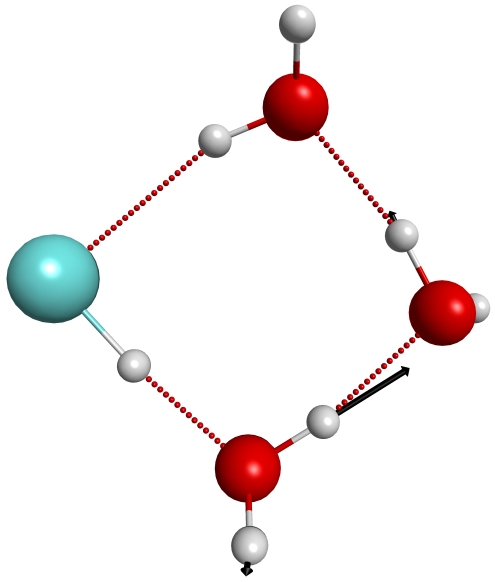

Figure 3.1: The global minimum configuration of $HCl{-}(H_2O)_3$. Arrows depict the vector motion of the O−H stretch mode used for excitation in this study.

$$HCl{-}(H_2O)_3 \longrightarrow HCl + (H_2O)_3 \tag{3.1}$$

$$HCl{-}(H_2O)_3 \longrightarrow H_2O + HCl{-}(H_2O)_2 \tag{3.2}$$

An open question is whether the final trimer products, $(H_2O)_3$ (WWW) and $HCl{-}(H_2O)_2$ (HWW), have cyclic or open-chair configurations. The cyclic forms of these trimers are more stable energetically; however, the transition states required for their formation via VP of the tetramer are tight and thus disfavored by entropy. The theoretical examination presented here strives to answer this intriguing question.

The investigation of the VP of the HWWW tetramer poses challenges for theory, requiring an accurate potential energy surface (PES) that describes the complex at the high energies of dissociation to the two product channels of interest here. (The need to run thousands of trajectories for roughly 10 picoseconds rules out an *ab initio* direct dynamics approach.) Here the PES employed is based on high-level *ab initio* many-body components, as described in detail and tested previously by Mancini and Bowman.[81] Structures were optimized and vibrational frequencies were determined

using different approximations. Previous calculations for dimers and trimers gave H-bond dissociation energies that were in close agreement with experiments. These studies are summarized in recent papers and review articles.[83–88] In addition, quasi-classical trajectory calculations performed on these highly-accurate PESs were used successfully before to determine the VP dynamics and dissociation energies of $(H_2O)_2$, HCl−H_2O, $(H_2O)_3$, and $(HCl)_3$.[83,84,86–88]

In this chapter, the results of a theoretical study of the predissociation of HWWW via Pathways 1 and 2 was presented. We report our best theoretical estimates for the dissociation energies for Pathways 1 and 2, rotational energy distributions for the HCl and H_2O monomer fragments, and fragment speed distributions. Moreover, we gain deeper insight into the predissociation dynamics by analyzing dissociative trajectories, obtained by QCT calculations, for the two dissociation pathways. These indicate that cyclic trimer fragments are formed in the two pathways, and the dissociation mechanism follows trends congruent with smaller neutral cluster works.

3.2 Theoretical methods and energetics

As noted above, the PES used was a highly accurate many-body potential constructed by Mancini and Bowman.[81] Accurate dissociation energies for numerous dissociation pathways, including the high energy breakup to H+W+W+W, were calculated using D_e values from complete basis set (CBS) calculations and zero-point energies (ZPE) using an unbiased diffusion Monte Carlo (DMC) method for the HWWW tetramer and various product fragments.

Table 3.1 lists benchmark dissociation enegies for relevant products. H-bond dissociation energies were calculated using D_e value of complete basis set (CBS), and ZPE values using the unweighted diffusion Monte Carlo (DMC) method for HCl−$(H_2O)_3$ and various product fragments. The CBS calculations were performed at the CCSD(T)/aVTZ/aVQZ level of theory with L3 extrapolation for the corre-

lation energy and Karton-Martin extrapolation for the Hartree-Fock energy, using MOLPRO 2010. The DMC caclulations were performed using 4000 walkers and a step size of 2.5 imaginary time units. Those trajectories were first equilibrated for 2000 steps and then propagated for at least 24000 steps. The uncertainties were measured by first block averaging the trajectories in sections of 4000 time steps, and then computing the standard deviation of the block averages. The excitation energy in the QCT calculations is 3550 cm^{-1}, which means that only Pathways 1 (2426 $\pm$ 23) and 2 (2826 $\pm$ 19 cm^{-1}) are feasible.

Fragments	D_e, cm^{-1}	D_0, cm^{-1}
$(H_2O)_3 + (HCl)$	3008	2426 $\pm$ 23
$(H_2O)_2(HCl) + (H_2O)$	3634	2826 $\pm$ 19
$(H_2O)_2 + (H_2O)(HCl)$	4866	3794 $\pm$ 18
$(H_2O)(HCl) + (H_2O) + (H_2O)$	6623	4907 $\pm$ 18
$(H_2O)_2 + (H_2O) + (HCl)$	6802	5174 $\pm$ 17
$(H_2O) + (H_2O) + (H_2O) + (HCl)$	8559	6287 $\pm$ 17

Table 3.1: Summary of benchmark dissociation energies

The VP dynamics reported here are based on QCT calculations very similar to those reported previously,[83,84] so we only describe them briefly. The trajectories were initiated at the global minimum configuration of HWWW, depicted in Figure 3.1, and assignment of harmonic ZPE for each mode followed by exciting the mode of interest. From the normal mode analysis (NMA) using the PES (see Table 3.2), one of the O−H stretch modes, depicted in Figure 3.1, whose frequency is only 20 cm^{-1} higher than the experimental energy, was the mode excited in this study.

After the total vibrational energy was assigned, an ensemble of trajectories was generated by randomly distributing the normal mode displacement and momentum for each mode. The following is the classical trajectory setup procedure.[89] Then the normal coordinates and momenta were transformed into Cartesian counterparts. During the transformation, small spurious angular momentum was generated and then removed so that the total angular momentum was zero. The removal of rotational

Mode	Frequency, cm^{-1}	Mode	Frequency, cm^{-1}	Mode	Frequency, cm^{-1}
1	30	10	304	19	1667
2	61	11	379	20	1683
3	136	12	412	21	2376
4	170	13	499	22	3570
5	182	14	636	23	3660
6	218	15	713	24	3749
7	225	16	743	25	3889
8	252	17	908	26	3896
9	287	18	1655	27	3914

Table 3.2: The table shows vibrational normal modes generated using the PES. The vibrational levels are heavily coupled, and it is not easy to assign clear motion to each one. The density of states is higher than in the trimer or dimer, and it is expected that relaxation between modes occurs much faster. Mode 22 at 3570 cm^{-1} is the mode chosen for excitation, and it is predominantly an H-bonded OH-stretch vibration, which has a large oscillator strength (See Figure 3.1).

energy resulted in a loss of total energy, so the iteration was corrected by a scaling step to increase harmonic displacement and momenta to compensate for the energy loss. Finally, the total energy was the sum of the anharmonic ZPE (17683 cm^{-1}), calculated using DMC, and the excitation energy used in the experiment (3550 cm^{-1}), 21233 cm^{-1}. Trajectories were then propagated using a velocity-Verlet algorithm with a step size of 0.06 fs and terminated when any individual bond length exceeded 16 Å. The total energy of the trajectories was roughly seven times larger than the PES D_e for either pathway, leading to relatively prompt dissociation (see below); however, as expected, many trajectories resulted in products with less energy than the ZPE, as discussed in more detail below.

Final product channels were categorized by the distance between the monomers. The HWWW complex dissociates classically into numerous products, of which only those in Pathways 1 and 2 are rigorously open when considering ZPE of the fragments (Table 3.1). Thus, distances between all possible fragments were monitored and the products of a dissociated trajectory were identified based on the condition that the shortest intermolecular distance between one monomer and other fragments was

greater than 6.5 Å. Overall, 48885 trajectories were run, of which 15242 dissociated to Pathway 1 and 19838 to Pathway 2, with no consideration of ZPE of the fragments. We return to this branching ratio in the next section. The average termination time for both channels was approximately 7 ps. Note that the remaining configurations belong to other dissociation products are discarded because these channels have D_0 values higher than the excitation energy (see Table 3.1), making them rigorously energetically forbidden. As a result, it is safe to say that the HCl fragment comes only from Pathway 1, and the water fragment only from Pathway 2.

The analysis of the fragments' internal energies was done in the standard way.[89] Specifically, for each trajectory corresponding to Pathway 1 the magnitude of the classical angular momentum of HCl (in atomic units), $\boldsymbol{j}$, was obtained. From this, J was obtained from $|\boldsymbol{j}|^2 = J(J+1)$ and rounded to the nearest integer. The same procedure was applied to obtain J for the H_2O product following Pathway 2. Then, the angular momenta were removed so that the remaining energy was the vibrational energy, and the difference with the total internal energy was the rotational energy. In this way, the vibrational and rotational energies of the fragments were obtained. The center-of-mass translational energy, E_t, was calculated directly using $E_t = \frac{1}{2}mv^2$, where m is the reduced mass of the two fragments and v is the relative speed. Standard histogram binning was done for the HCl and H_2O rotations. For the H_2O fragments, the corresponding J was obtained similarly as for HCl, and then J_{K_a,K_c} states were determined by binning QCT rotational energies to the corresponding experimental rotational energies. As noted above, most of the fragments were formed with energy less than the ZPE. Thus several standard constraints were applied by comparing the calculated vibrational energy to the DMC-calculated ZPE of the fragments. The "soft ZPE constraint" requires

$$E_{vib}(\mathrm{HCl{-}(H_2O)_2}) + E_{vib}(\mathrm{H_2O}) > ZPE(\mathrm{HCl{-}(H_2O)_2}) + ZPE(\mathrm{H_2O}) \tag{3.3}$$

in Pathway 2 or

$$E_{vib}((H_2O)_3\ ) + E_{vib}(HCl) > ZPE((H_2O)_3\ ) + ZPE(HCl) \tag{3.4}$$

in Pathway 1, while the "hard ZPE constraint" requires each fragment to have a vibrational energy greater than the ZPE of the fragment. Lastly, we consider a "hard ZPE on monomer" or "monomer only ZPE", which requires only the dissociated water or HCl to satisfy the ZPE condition. Ideally, the hard ZPE constraint should be applied; however, this is problematic in the present case, because it results in the rejection of such a large number of trajectories that final conditions such as rotational distributions are statistically highly uncertain.

3.3 Results and discussion

3.3.1 Fragment Speed Distributions

Figure 3.2 and Figure 3.3 shows calculated speed distributions of the HCl fragment in $J = 4$ and $J = 6$ computed by using the ZPE constraints described in the main text. The number of trajectories for different ZPE constraints of $J = 4$ and $J = 6$ are presented in Table 3.3.

	No Constraint	HCl-only ZPE	Soft ZPE	Hard ZPE
$J = 4$	2465	601	2381	345
$J = 6$	1536	405	1422	171

Table 3.3: Number of collected trajectories using different ZPE constraints for Pathway 1.

When using soft ZPE constraints, a significant number of trajectories are collected, while using hard ZPE constraint filters out a large portion of all trajectories, providing poor statistics. For $J = 4$, the cutoff speed of the soft ZPE constraint is 670 m/s, while for the hard ZPE constraint it is 605 m/s. For $J = 6$, the corresponding soft and hard ZPE cutoffs are 601 and 581 m/s. As expected, the cutoff speed for $J = 6$ is lower than for $J = 4$.

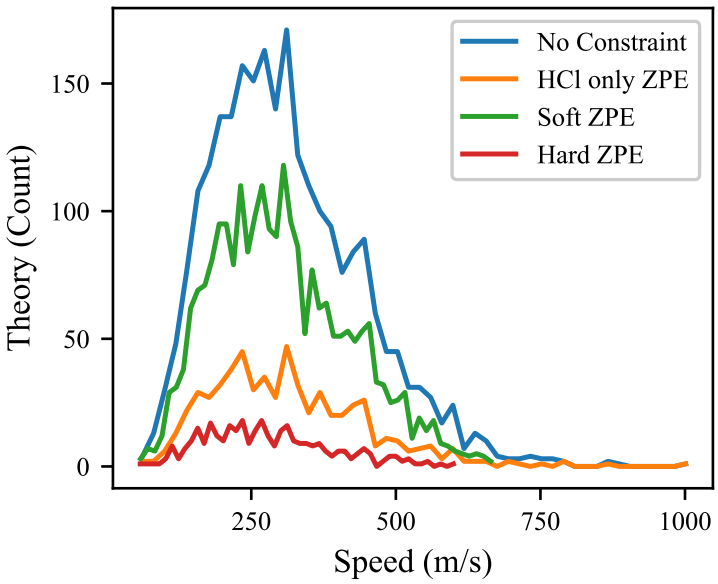

Figure 3.2: Theoretical speed distributions for the HCl monomers in rotational level $J = 4$ following Pathway 1.

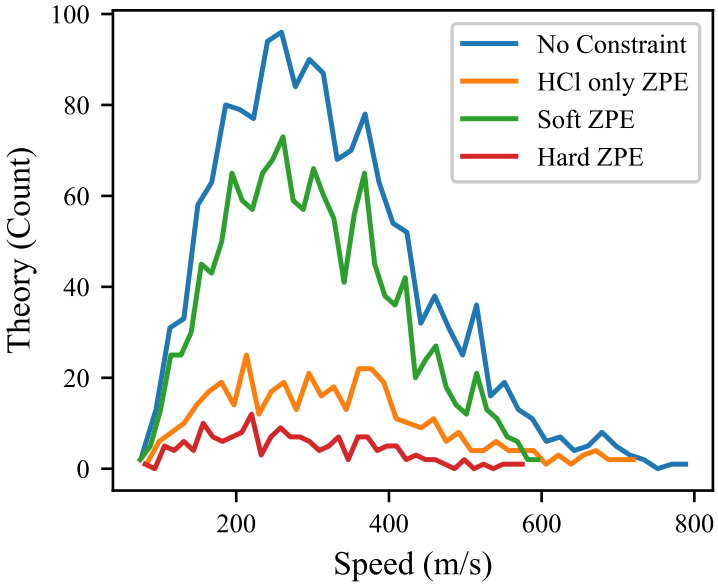

Figure 3.3: Theoretical speed distributions for the HCl monomers in rotational level $J = 6$ following Pathway 1.

	Peak Position (m/s)	Average Speed (m/s)	Average E_t (cm^{-1})
$J = 4$	260	303	364
$J = 6$	210	297	250

Table 3.4: Theoretical values (soft ZPE) for approximate peak positions, average speed of the HCl fragment and average translational energy E_t for Pathway 1.

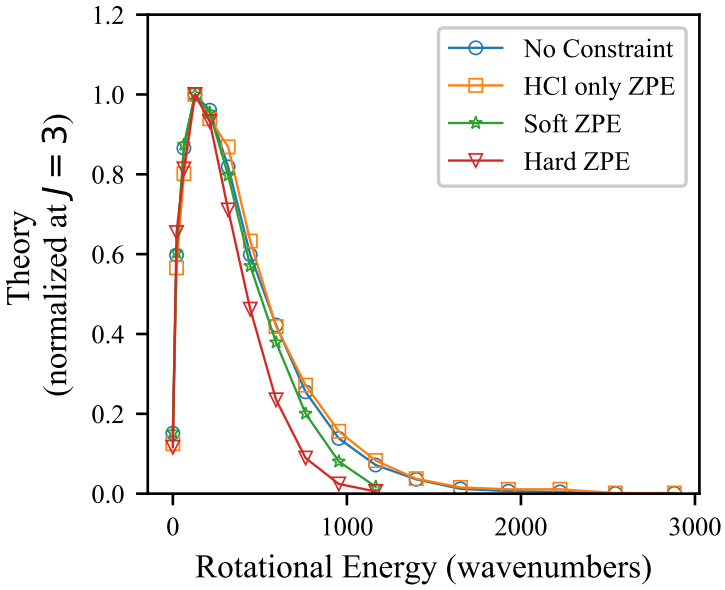

Figure 3.4: Comparison between calculated rotational populations for the HCl monomer following dissociation of HWWW with indicated constraints. The discrete rotational energy data points for each constraint in the calculations are connected by a line for visual guidance. The populations are normalized to $J = 3$.

3.3.2 Fragment Rotational Energy Distributions

Figure 3.4 shows the relative rotational state populations plotted as a function of rotational energy along with calculated rotational energy distributions. The hard and soft ZPE constraints both show that the rotational energy cut-offs correspond to $J = 10$ in the HCl monomer fragment.

The calculated rotational energy distributions for the water fragment following Pathway 2 are shown in Figure 3.5. A total of 1058 trajectories with a hard ZPE constraint and 14223 with a soft ZPE constraint produced rotational energy maxima of 760 cm^{-1} and 1011 cm^{-1}, respectively. With the theoretically calculated D_0, the

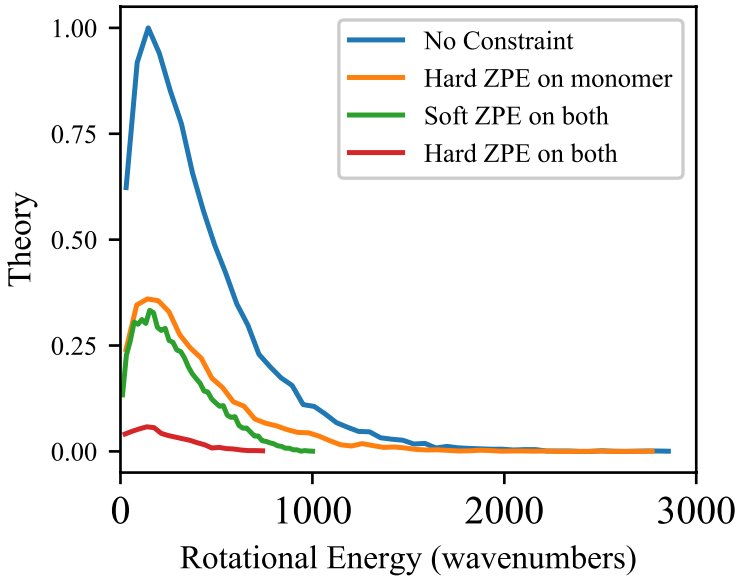

Figure 3.5: Water monomer rotational energy distributions for Pathway 2 calculated using the indicated constraints.

expected rotational cut-off should be 724 cm^{-1} by conservation of energy. The cut-off of rotational energy under both soft and hard ZPE obeys this theoretical upper limit with the closest match coming from the hard ZPE constraint.

3.3.3 Dissociative Trajectories and Lifetimes

Examination of dissociative trajectories can shed light on mechanisms; snapshots from two representative trajectories are shown in Figure 3.6 and Figure 3.7. As stated above, the calculated dissociation energies for both pathways correspond to cyclic trimer fragments. Indeed, it is evident from Figure 3.6 and 3.7 that just prior to dissociation, the polyatomic fragments form cyclic structures, sometimes with the monomer fragment still attached to the trimer ring by a hydrogen bond. In fact, the product water trimer ring breaks and reform many times during the dissociation until the monomer (HCl or H_2O) eventually separates, and there are many intermediate structures seen in each trajectory. No low-energy open-chain stable trimer fragments were found in the calculations, and we conclude that the VP products are a monomer

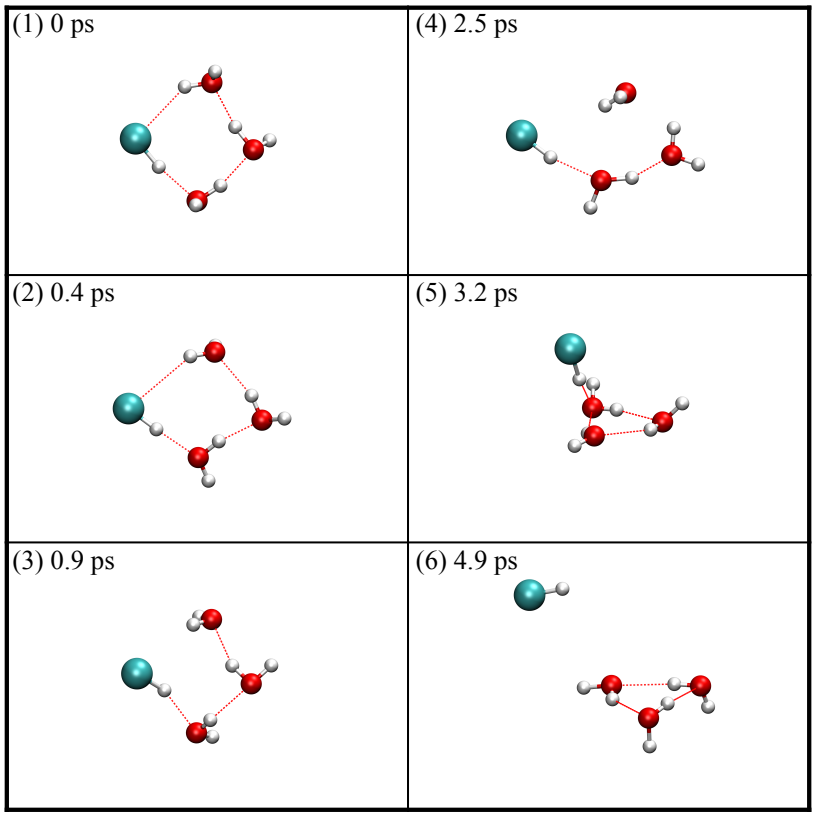

Figure 3.6: Trajectory snapshots of Pathway 1 for $J = 4$ ($\sim$ 6 ps)

and a cyclic fragment. The fragments may evolve via intermediates that have the monomer H-bonded to the cyclic trimer, as seen for example in the HCl trajectory in Figure 3.6. The multiple break-up and formation of H-bonds appear to be a common motif in the VP of small clusters, which has been seen in trajectories of VP of $(H_2O)_2$, $(H_2O)_3$ and $(HCl)_3$.[83,86–88]

The vibrational predissociation lifetimes for the HWWW tetramer are significantly shorter than that of smaller cluster systems. Both pathways show lifetimes of about 7 ps, compared to the water trimer (84% dissociated at 10.5 ps) and the water dimer (84% dissociated at 25 ps).[83,86] Based solely on cluster size, the trend is that larger clusters have shorter dissociation lifetimes. This trend may be explained partly by the time it takes for the initial OH-stretch excitation to couple to low-energy intermolecular vibrational levels of the cluster. For example, the lifetime of the HCl trimer is much longer than that of the H_2O trimer, because of the existence of a bending

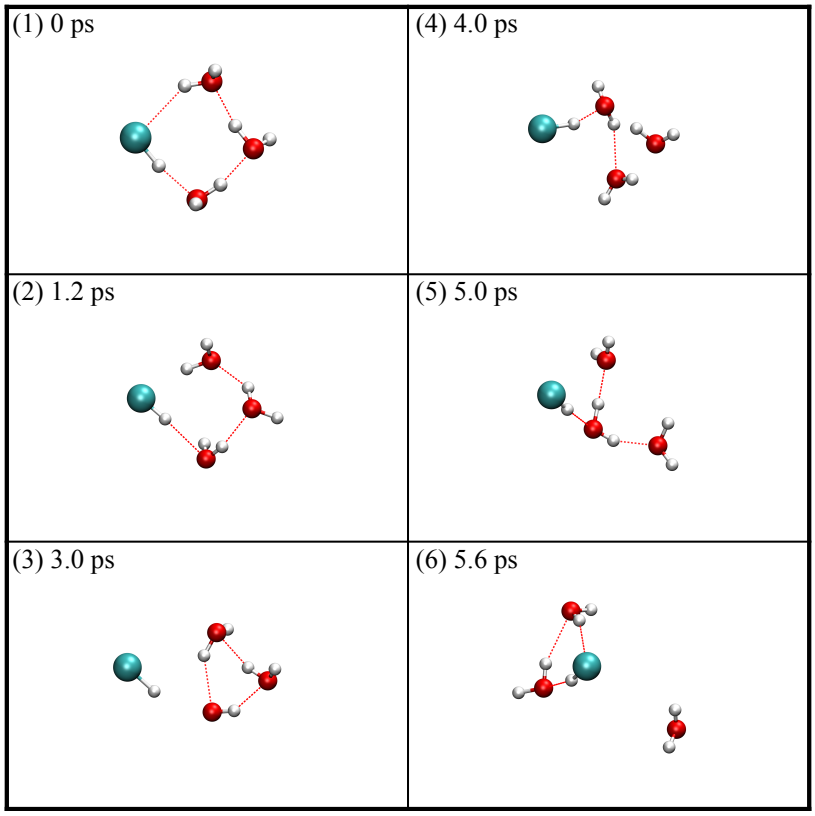

Figure 3.7: Trajectory snapshots of Pathway 2 for $J_{K_a,K_c} = 2_{2,1}$ ($\sim$ 7 ps).

mode in the water monomer, which facilitates coupling to the intermolecular modes in the latter.[83,87,88] The lifetime of > 1 ns for the HCl trimer is indeed correlated with the persistence of its coupled HCl stretch modes.[88] In the present work, the excited H-bonded OH-stretch of the tetramer is likely to couple more efficiently to the intermolecular modes than in the water trimer because of the higher density of states of intermolecular modes in the tetramer. Also, the nominal OH-stretch vibration has contributions from other motions, which may facilitate coupling. Therefore, it is reasonable that the lifetimes of larger clusters become shorter, though at some point the statistical nature of the predissociation process will cause the rates to decrease with cluster size. In large clusters, we expect that energy disposition would be more statistical-like, although because of the relatively large energy separation between the rotational levels of the HCl monomer, some deviations from statistical behavior would not be surprising. Overall, however, the VP of HWWW is typical of that of neutral clusters, exhibiting no sign of impending ionization.

The branching ratio for the two pathways can be obtained from the QCT calculations; however, the results are very sensitive to the ZPE constraint used, as expected. With no ZPE constraint, the branching ratio for Pathway 1 to 2 is 0.77 to 1, with the soft ZPE constraint it is 0.99 to 1 and with the hard ZPE constraints it is 1.76 to 1. With the hard ZPE constraints and using the calculated values of D_0 for the two pathways, the excess energy for Pathway 1 is 1124 cm^{-1} (3550-2426 cm^{-1}) and for Pathway 2 it is 724 cm^{-1} (3550-2826 cm^{-1}) – a difference of roughly 400 cm^{-1}. However, for the PES the difference is 500 cm^{-1}, owing to the differences in the PES D_e and the CBS values. In any case, the difference in energy certainly favors Pathway 1 over Pathway 2. However, without the ZPE constraint Pathway 2 is slightly favored even though the difference in electronic energies is even larger, namely 600 cm^{-1} from the CBS values and 700 cm^{-1} from the PES values. Naively, there are three ways to eliminate a water monomer and only one way to eliminate HCl, which would lead

to a branching ratio of 0.33 to 1 if the two channels were isoenergetic. This ratio is not observed, even without any ZPE constraint, suggesting that the branching ratio is not a simple statistical one.

3.4 Summary and conclusions

The VP of cyclic HWWW, the largest HCl$-(H_2O)_n$ cluster that is not ionized, has been investigated by theory. The cluster was excited in the H-bonded OH stretch fundamental and HCl and H_2O have been identified as the products of Pathways 1 and 2, respectively. Calculations show that these pathways terminate in the corresponding cyclic products, WWW and HWW, and their D_0 values are 2426 $\pm$ 23 cm^{-1} and 2826 $\pm$ 19 cm^{-1}, respectively.

Trajectory calculations show that the dissociation lifetime is considerable and during each trajectory, terminating in either HCl or H_2O monomer fragments, H-bonds are broken and reformed many times, until the monomer detaches completely, leaving a cyclic trimer as the cofragment. Such behavior is typical in the VP of other small clusters of HCl and/or H_2O, where the rate limiting step is often the initial coupling of the excited OH or HCl stretch vibration to other intramolecular and intermolecular vibrations of the cluster, followed by energy randomization in the excited cluster and finally dissociation.

Except for the branching ratios of Pathways 1 and 2, which are calculated to be non-statistical, energy partitioning in the other degrees of freedom appear statistical-like, as it is typical of clusters with a high density of vibrational states. Overall, the VP of the HWWW is typical of that of other neutral clusters of comparable size, and does not show evidence of impending ionization.

Chapter 4 Summary

In this thesis, I presented applications of potential energy surfaces by examining three different molecular systems.

In Chapter 2, an accurate, full-dimensional, 2-body potential energy surface for CO_2-H_2O is constructed. This 2-body PES, combined with previously existing monomer PESs, gives an accurate description for flexible CO_2-H_2O system. This PES provides an efficient model to evaluate the properties of the dimer. For example, the benchmark D_0 is evaluated to be 758 cm^{-1} by running DMC with PES and using the existing benchmark D_e. In addition, by performing VSCF/VCI coupled-mode calculations, vibrational fundamentals for CO_2-H_2O were reported and they match well with spectrum data, which is another testimony of the usefulness of an accurate and efficient PES.

The power of this 2-body PES can be greatly enhanced by adding more many-body interactions. As shown in the Chapter 2, this PES can be used to simulate small CO_2 hydrate clathrate $CO_2@(H_2O)_{20}$ by including water potential. As a result, some important properties such as D_e or fundamentals are obtained thanks to the efficiency of PES.

However, as for the CO_2 hydrate clathrate system, there is still much to be done. In order to be more accurate to describe CO_2 hydrate clathrate system, $CO_2-H_2O-H_2O$ 3-body interaction may be important to include in certain circumstances. In addition, it is still an open question how to evaluate so many interactions of CO_2 hydrate clathrate efficiently without too much sacrifice of accuracy.

In Chapter 3, a QCT study of cyclic $HCl-(H_2O)_3$ is presented, using an existing PES. The large number of trajectories required by QCT calculation can be finished by taking advantage of the efficiency of PES. The PES helps calculate many important

properties related to VP, such as dissociation energy and branching ratio. However, it is acknowledged that this analytical PES can be less accurate and even with unpredictable extreme behaviors if the geometry of molecule is away from equilibrium. It remains an important and interesting question how PES can overcome such instability in the future.

Bibliography

[1] Wang, Q. K.; Bowman, J. M. *J. Chem. Phys.* **2017**, *147*, 161714.

[2] Brooks, B. R. et al. *J. Comp. Chem.* **2009**, *30*, 1545–1614.

[3] Ponder, J. W.; Wu, C.; Ren, P.; Pande, V. S.; Chodera, J. D.; Schnieders, M. J.; Haque, I.; Mobley, D. L.; Lambrecht, D. S.; DiStasio, R. A.; Head-Gordon, M.; Clark, G. N. I.; Johnson, M. E.; Head-Gordon, T. *J. Phys. Chem. B* **2010**, *114*, 2549–2564.

[4] van Duin, A. C. T.; Dasgupta, S.; Lorant, F.; Goddard, W. A. *J. Phys. Chem. A* **2001**, *105*, 9396–9409.

[5] Braams, B. J.; Bowman, J. M. *Int. Rev. Phys. Chem.* **2009**, *28*, 577–606.

[6] Bowman, J. M.; Czako, G.; Fu, B. *Phys. Chem. Chem. Phys.* **2011**, *13*, 8094–8111.

[7] Behler, J. *Phys. Chem. Chem. Phys.* **2011**, *13*, 17930–17955.

[8] Jiang, B.; Li, J.; Guo, H. *Int. Rev. Phys. Chem.* **2016**, *35*, 479–506.

[9] Bukowski, R.; Szalewicz, K.; Groenenboom, G. C.; van der Avoird, A. *Science* **2007**, *315*, 1249–1252.

[10] Wang, Y.; Huang, X.; Shepler, B. C.; Braams, B. J. *J. Chem. Phys.* **2011**, *134*, 94509.

[11] Babin, V.; Medders, G. R.; Paesani, F. *J. Chem. Theory Comput.* **2014**, *10*, 1599–1607.

[12] Homayoon, Z.; Conte, R.; Qu, C.; Bowman, J. M. *J. Chem. Phys.* **2015**, *143*, 84302.

[13] Qu, C.; Conte, R.; Houston, P. L.; Bowman, J. M. B. *Phys. Chem. Chem. Phys.* **2015**, *17*, 8172–8181.

[14] Conte, R.; Qu, C.; Bowman, J. M. *J. Chem. Theory Comput.* **2015**, *11*, 1631–1638.

[15] Chaban, G. M.; Bernstein, M.; Cruikshank, D. P. *Icarus* **2007**, *187*, 592–599.

[16] Miller, S. L.; Smythe, W. D. *Science* **1970**, *170*, 531–533.

[17] Lambert, R. S. J.; Chamberlanin, V. E. *Icarus* **1978**, *34*, 568–580.

[18] Hoffman, N. *Icarus* **2000**, *146*, 326–342.

[19] Radhakrishnan, R.; Trout, B. L. *J. Chem. Phys.* **2002**, *117*, 1786.

[20] Park, Y.; Kim, D.-Y.; Lee, J.-W.; Huh, D.-G.; Park, K.-P.; Lee, J.; Lee, H. *Proc. Natl. Acad. Sci. U. S. A.* **2006**, *103*, 12690–12694.

[21] Velaga, S. C.; Anderson, B. J. *J. Phys. Chem. B* **2014**, *118*, 577–589.

[22] Peterson, K. I.; Klemperer, W. *J. Chem. Phys.* **1984**, *80*, 2439.

[23] Tso, T.-L.; Lee, E. K. C. *J. Phys. Chem.* **1985**, *89*, 1612–1618.

[24] Schriver, A.; Schriver-Mazzuoli, L.; Chaquin, P.; Dumont, E. *J. Phys. Chem. A* **2006**, *110*, 51–56.

[25] Zhu, Y.; Li, S.; Sun, P.; Duan, C. *J. Mol. Spectrosc.* **2013**, *283*, 7–9.

[26] Jönsson, B.; Karlström, G.; Wennerström, H. *Chem. Phys. Lett.* **1975**, *30*, 58–59.

[27] Fredin, L.; Nelander, B.; Ribbergard, G. *Chem. Sripta* **1975**, *7*, 11–13.

[28] Zhang, N. R.; Shillady, D. D. *J. Chem. Phys.* **1994**, *100*, 5230.

[29] Sadlej, J.; Makarewicz, J.; Chałasiński, G. *J. Chem. Phys.* **1998**, *109*, 3919–3927.

[30] Tso, T.-L.; Lee, E. K. C. *J. Phys. Chem.* **1985**, *89*, 1618–1631.

[31] Danten, Y.; Tassaing, T.; Besnard, M. *J. Phys. Chem. A* **2005**, *109*, 3250–3256.

[32] Wilcox, C. F.; Bauer, S. H. *Mol. Phys.* **2005**, *103*, 2829–2837.

[33] Altmann, J. A.; Ford, T. A. *J. Mol. Struct. THEOCHEM* **2007**, *818*, 85–92.

[34] Makarewicz, J. *J. Chem. Phys.* **2010**, *132*, 234305.

[35] de Lange, K. M.; Lane, J. R. *J. Chem. Phys.* **2011**, *134*, 034301.

[36] Wheatley, R. J.; Harvey, A. H. *J. Chem. Phys.* **2011**, *134*, 134309.

[37] Makarewicz, J.; Ha, T.-K.; Bauder, A. *J. Chem. Phys.* **1993**, *99*, 3694.

[38] Xie, Z.; Bowman, J. M. *J. Chem. Theory Comput.* **2010**, *6*, 26–34.

[39] Partridge, H.; Schwenke, D. *J. Chem. Phys.* **1997**, *106*, 4618–4639.

[40] Huang, X.; Schwenke, D. W.; Tashkun, S. A.; Lee, T. J. *J. Chem. Phys.* **2012**, *136*, 124311.

[41] Adler, T. B.; Knizia, G.; Werner, H.-J. *J. Chem. Phys.* **2007**, *127*, 221106.

[42] Knizia, G.; Adler, T. B.; Werner, H.-J. *J. Chem. Phys.* **2009**, *130*, 54104.

[43] Werner, H.-J.; Knowles, P. J.; Knizia, G.; Manby, F. R.; Schütz, M.; Others, MOLPRO, version 2010.1, a package of ab initio programs. 2010.

[44] Dunning Jr, T. H. *J. Chem. Phys.* **1989**, *90*, 1007.

[45] E. Woon, D.; Dunning Jr, T. H. *J. Chem. Phys.* **1994**, *100*, 2975.

[46] Anderson, J. B. *J. Chem. Phys.* **1975**, *63*, 1499.

[47] Anderson, J. B. *J. Chem. Phys.* **1976**, *65*, 4121.

[48] McCoy, A. B. *Int. Rev. Phys. Chem.* **2006**, *25*, 77–107.

[49] Bowman, J. M.; Schafer, P. *J. Mol. Struct.* **1990**, *224*, 133–139.

[50] Christoffel, K. M.; Bowman, J. M. *J. Chem. Phys.* **1996**, *104*, 8348.

[51] Shank, A.; Wang, Y.; Kaledin, A.; Braams, B. J.; Bowman, J. M.; Shank, A.; Wang, Y.; Kaledin, A.; Braams, B. J.; Bowman, J. M. *J. Chem. Phys.* **2009**, *130*, 144314.

[52] Carter, S.; Culik, S. J.; Bowman, J. M. *J. Chem. Phys.* **1997**, *107*, 10458–10469.

[53] Carter, S.; Bowman, J. M.; Handy, N. C. *Theor. Chem. Acc.* **1998**, *100*, 191–198.

[54] Carter, S.; Bowman, J. M. *J. Chem. Phys.* **1998**, *108*, 4397.

[55] Carter, S.; Handy, N. C. *J. Chem. Phys.* **2000**, *113*, 987.

[56] Bowman, J. M.; Carter, S.; Huang, X. *Int. Rev. Phys. Chem.* **2003**, *22*, 533–549.

[57] Bowman, J. M. *Acc. Chem. Res* **1986**, *19*, 202–208.

[58] Valdés, Á.; Arismendi-Arrieta, D. J.; Prosmiti, R. *J. Phys. Chem. C* **2015**, *119*, 3945–3956.

[59] Liang, S.; Liang, D.; Wu, N.; Yi, L.; Hu, G. *J. Phys. Chem. C* **2016**, *120*, 16298–16304.

[60] Srivastava, H. K.; Sastry, G. N. *J. Phys. Chem. A* **2011**, *115*, 7633–7637.

[61] Qu, C.; Bowman, J. M. *J. Phys. Chem. C* **2016**, *120*, 3167–3175.

[62] Wang, Y.; Bowman, J. M. *J. Chem. Phys.* **2011**, *134*, 154510.

[63] Columberg, G.; Bauder, A.; Heineking, N.; Stahl, W.; Makarewicz, J. *Mol. Phys.* **1998**, *93*, 215–228.

[64] Soulard, P.; Tremblay, B. *J. Chem. Phys.* **2015**, *143*, 224311.

[65] Zhang, X.; Sander, S. P. *J. Phys. Chem. A* **2011**, *115*, 9854–9860.

[66] Sum, A. K.; Burruss, R. C.; Sloan, E. D. *J. Phys. Chem. B* **1997**, *101*, 7371–7377.

[67] Oancea, A.; Grasset, O.; Le Menn, E.; Bollengier, O.; Bezacier, L.; Le Mouélic, S.; Tobie, G. *Icarus* **2012**, *221*, 900–910.

[68] Zuraski, K.; Kwasniewski, D.; Samanta, A. K.; Reisler, H. *J. Phys. Chem. Lett.* **2016**, *7*, 4243–4247.

[69] Scheiner, S. *Noncovalent forces*; Springer, 2015; Vol. 19.

[70] Bondybey, V. E.; Beyer, M.; Achatz, U.; Joos, S.; Niedner-Schatteburg, G. *Isr. J. Chem.* **1999**, *39*, 213–219.

[71] Masia, M.; Forbert, H.; Marx, D. *J. Phys. Chem. A* **2007**, *111*, 12181–12191.

[72] Forbert, H.; Masia, M.; Kaczmarek-Kedziera, A.; Nair, N. N.; Marx, D. *J. Am. Chem. Soc.* **2011**, *133*, 4062–4072.

[73] Andot, K.; Hynes, J. T. *J. Mol. Liq.* **1995**, *64*, 25–37.

[74] Sugawara, S.; Yoshikawa, T.; Takayanagi, T.; Tachikawa, M. *Chem. Phys. Lett.* **2011**, *501*, 238–244.

[75] Chaban, G. M.; Gerber, R. B.; Janda, K. C. *J. Phys. Chem. A* **2001**, *105*, 8323–8332.

[76] Mancini, J. S.; Bowman, J. M. *Phys. Chem. Chem. Phys.* **2015**, *17*, 6222–6226.

[77] Vargas-Caamal, A.; Cabellos, J. L.; Ortiz-Chi, F.; Rzepa, H. S.; Restrepo, A.; Merino, G. *Chem. Eur. J.* **2016**, *22*, 2812–2818.

[78] Guggemos, N.; Slavíček, P.; Kresin, V. V. *Phys. Rev. Lett.* **2015**, *114*, 43401.

[79] Packer, M. J.; Clary, D. C. *J. Phys. Chem.* **1995**, *99*, 14323–14333.

[80] Bacelo, D. E.; Binning, R. C.; Ishikawa, Y. *J. Phys. Chem. A* **1999**, *103*, 4631–4640.

[81] Mancini, J. S.; Bowman, J. M. *J. Phys. Chem. Lett.* **2014**, *5*, 2247–2253.

[82] Odde, S.; Mhin, B. J.; Lee, S.; Lee, H. M.; Kim, K. S. *J. Chem. Phys.* **2004**, *120*, 9524–9535.

[83] Samanta, A. K.; Wang, Y.; Mancini, J. S.; Bowman, J. M.; Reisler, H. *Chem. Rev.* **2016**, *116*, 4913–4936.

[84] Samanta, A. K.; Czako, G.; Wang, Y.; Mancini, J. S.; Bowman, J. M.; Reisler, H. *Acc. Chem. Res.* **2014**, *47*, 2700–2709.

[85] Rocher-Casterline, B. E.; Mollner, A. K.; Ch'ng, L. C.; Reisler, H. *J. Phys. Chem. A* **2011**, *115*, 6903–6909.

[86] Ch'ng, L. C.; Samanta, A. K.; Czako, G.; Bowman, J. M.; Reisler, H. *J. Am. Chem. Soc.* **2012**, *134*, 15430–15435.

[87] Ch'ng, L. C.; Samanta, A. K.; Wang, Y.; Bowman, J. M.; Reisler, H. *J. Phys. Chem. A* **2013**, *117*, 7207–7216.

[88] Mancini, J. S.; Samanta, A. K.; Bowman, J. M.; Reisler, H. *J. Phys. Chem. A* **2014**, *118*, 8402–8410.

[89] Hase, W. L. *Encycl. Comput. Chem.*; American Cancer Society, 2002.